frontiers | Frontiers in Complex Systems

TYPE Original Research
PUBLISHED 20 November 2023
DOI 10.3389/fcpxs.2023.1281714

OPEN ACCESS

EDITED BY
Byungjoon Min,
Chungbuk National University, Republic of Korea

REVIEWED BY
Flaviano Morone,
New York University, United States
Wei Wang,
Chongqing Medical University, China

*CORRESPONDENCE
Elkaïoum M. Moutuou,
elkaioum.moutuou@concordia.ca

RECEIVED 22 August 2023
ACCEPTED 19 October 2023
PUBLISHED 20 November 2023

CITATION
Moutuou EM, Ali OBK and Benali H (2023), Topology and spectral interconnectivities of higher-order multilayer networks.
Front. Complex Syst. 1:1281714.
doi: 10.3389/fcpxs.2023.1281714

Topology and spectral interconnectivities of higher-order multilayer networks

Elkaïoum M. Moutuou[1]*, Obaï B. K. Ali[2] and Habib Benali[3]

[1]PERFORM Centre, Concordia University, Montreal, QC, Canada, [2]Department of Physics, Gina Cody School of Engineering and Computer Science, Concordia University, Montreal, QC, Canada, [3]Department of Electrical and Computer Engineering, Concordia University, Montreal, QC, Canada

Multilayer networks have permeated all areas of science as an abstraction for interdependent heterogeneous complex systems. However, describing such systems through a purely graph-theoretic formalism presupposes that the interactions that define the underlying infrastructures are only pairwise-based, a strong assumption likely leading to oversimplification. Most interdependent systems intrinsically involve higher-order intra- and inter-layer interactions. For instance, ecological systems involve interactions among groups within and in-between species, collaborations and citations link teams of coauthors to articles and *vice versa*, and interactions might exist among groups of friends from different social networks. Although higher-order interactions have been studied for monolayer systems through the language of simplicial complexes and hypergraphs, a systematic formalism incorporating them into the realm of multilayer systems is still lacking. Here, we introduce the concept of *crossimplicial multicomplexes* as a general formalism for modeling interdependent systems involving higher-order intra- and inter-layer connections. Subsequently, we introduce *cross-homology* and its spectral counterpart, the *cross-Laplacian* operators, to establish a rigorous mathematical framework for quantifying global and local intra- and inter-layer topological structures in such systems. Using synthetic and empirical datasets, we show that the spectra of the cross-Laplacians of a multilayer network detect different types of clusters in one layer that are controlled by hubs in another layer. We call such hubs spectral cross-hubs and define spectral persistence as a way to rank them, according to their emergence along the spectra. Our framework is broad and can especially be used to study structural and functional connectomes combining connectivities of different types and orders.

KEYWORDS

multilayer networks, cross-homology, multicomplexes, Laplacian, cross-hubs, spectral persistence

1 Introduction

Multilayer networks (De Domenico et al., 2013; Boccaletti et al., 2014; Kivelä et al., 2014) have emerged over the last decade as a natural instrument in modeling myriads of heterogeneous systems. They permeate all areas of science as they provide a powerful abstraction of real-world phenomena made of interdependent sets of units interacting with each other through various channels. The concepts and computational methods they purvey have been the driving force for recent progress in the understanding of many highly sophisticated structures such as heterogeneous ecological systems (Pilosof et al., 2017; Timóteo et al., 2018), spatiotemporal and multimodal human brain connectomes (Griffa

et al., 2017; Mandke et al., 2018; Pedersen et al., 2018), gene–molecule–metabolite interactions (Liu et al., 2020), and interdisciplinary scientific collaborations (Vasilyeva et al., 2021). This success has led to a growing interdisciplinary research investigating fundamental properties and topological invariants in multilayer networks.

Some of the major challenges in the analysis of a multilayer network are to quantify the *importance* and *interdependence* among its different components and subsystems, and describe the topological structures of the underlying architecture to better grasp the dynamics and information flow between its different network layers. Various approaches extending concepts, properties, and centrality indices from network science (Newman, 2003; Fortunato and Hric, 2016) have been developed, leading to tremendous results in many areas of science (Solá et al., 2013; Boccaletti et al., 2014; Sánchez-García et al., 2014; Flores and Romance, 2018; Timóteo et al., 2018; Wu et al., 2019; Liu et al., 2020; Yuvaraj et al., 2021). However, these approaches assume that inter- and intra-communications and relationships between the networks involved in such systems rely solely on node-based interactions. The resulting methods are, therefore, less insightful when the infrastructure is made up of higher-order *intra-* and *inter-connectivities* among node aggregations from different layers—as is the case for many phenomena. For example, heterogeneous ecosystems are made up of interactions among groups of the same or different species, social networks often connect groups of people belonging to different circles, and collaborations and citations form a higher-order multilayer network made of teams of co-authors interconnected to articles. Many recent studies have explored higher-order interactions and structures in monolayer networks (Benson et al., 2016; Iacopini et al., 2019; Lucas et al., 2020; Schaub et al., 2020; Bianconi, 2021) using different languages, such as *simplicial complexes* and *hypergraphs* (Shi et al., 2021; Young et al., 2021; Lotito et al., 2022; Majhi et al., 2022). However, a general mathematical formalism for modeling and studying higher-order multilayer networks is still lacking.

Our goal in this study is twofold. First, we propose a mathematical formalism that is rich enough to model and analyze multilayer complex systems involving higher-order connectivities within and in-between their subsystems. Second, we establish a unified framework for studying topological structures in such systems. This is performed by introducing the concepts of *crossimplicial multicomplex*, *cross-homology*, *cross-Betti vectors*, and *cross-Laplacians*. Before we dive deeper into these notions, we shall give the intuition behind them by considering the simple case of an undirected two-layered network Γ; here, Γ consists of two graphs (V_1, E_1) and (V_2, E_2), where V_1, V_2 are the node sets of Γ, $E_s \subseteq V_s \times V_s$, $s = 1, 2$ are the sets of intra-layer edges, and a set $E_{1,2} \subseteq V_1 \times V_2$ of *inter-layer edges*. Intuitively, Γ might be seen as a system of interactions between two networks. It means that the node set V_1 interacts not only with V_2 but also with the edge set E_2 and vice versa. Similarly, intra-layer edges in one layer interact with edges and triads in the other layer, and so on. This view suggests a more combinatorial representation by some kind of two-dimensional generalization of the fundamental notion of *simplicial complex* from algebraic topology (Mac Lane, 1963; Hatcher, 2000). The idea of *crossimplicial multicomplex* defined in the present work allows such a representation. In particular, when applied to a pairwise-based multilayer network, this concept allows to incorporate, on one hand, the *clique complexes* (Lim, 2020; Schaub et al., 2020) corresponding to the network layers, and on the other, the clique complex representing the inter-layer relationships between the different layers into one single mathematical object. Moreover, Γ can be regarded through different lenses, and each view displays different kinds of topological structures. The most naive perspective flattens the whole structure into a monolayer network without segregating the nodes and links from one layer or the other. Another viewpoint is of two networks with independent or interdependent topologies communicating with each other through the inter-layer links. The rationale for defining cross-homology and the cross-Laplacians is to view Γ as different systems, each with its own intrinsic topology but in which nodes, links, *etc.*, from one system have some restructuring power that allows them to impose and control additional topologies on the other. This means that in a multilayer system, a layer network might display different topological structures depending on whether we look at it from its own point of view, from the lens of the other layers, or as a part of a whole aggregated structure. We describe this phenomenon by focusing on the spectra and eigenvectors of the lower-degree cross-Laplacians. We shall, however, remark that our aim here is not to address a particular real-world problem but to provide broader mathematical settings that reveal and quantify the emergence of these structures in any type of multilayer network.

2 Crossimplicial multicomplexes

2.1 General definitions

Given two finite sets, V_1 and V_2, and a pair of integers $k, l \geq -1$, a (k, l)– *crossimplex* a in $V_1 \times V_2$ is a subset $\{v_0^1, \ldots, v_k^1, v_0^2, \ldots, v_l^2\}$ of $V_1^{k+1} \times V_2^{l+1}$, where $v_i^s \in V_s$ for $s = 1, 2$. The point v_i^1 (resp. v_j^2) is the *vertex* of a in V_1 (resp. V_2), and its *crossfaces* are its subsets of the form $\{v_0^1, \ldots, v_{i-1}^1, v_{i+1}^1, \ldots, v_k^1, v_0^2, \ldots, v_l^2\}$ for $0 \leq i \leq k$ and $\{v_0^1, \ldots, v_k^1, v_0^2, \ldots, v_{i-1}^2, v_{i+1}^2, \ldots, v_l^2\}$ for $0 \leq i \leq l$. Note that here we have used the conventions that $V_1^n \times V_2^0 = V_1^n$ and $V_1^0 \times V_2^n = V_2^n$.

An *abstract crossimplicial bicomplex* X (or a CSB) on V_1 and V_2 is a collection of crossimplices in $V_1 \times V_2$, which is closed under the inclusion of crossfaces, *i.e.*, the crossface of a crossimplex is also a crossimplex. A crossimplex is *maximal* if it is not the crossface of any other crossimplex. V_1 and V_2 are called the vertex sets of X.

Given a CSB X, for fixed integers $k, l \geq 0$, we denote, by $X_{k,l}$, the subset of all its (k, l)-crossimplices. We also use the notations $X_{0,-1} = V_1$, $X_{-1,0} = V_2$, and $X_{-1,-1} = \varnothing$. Recursively, $X_{k,-1}$ will denote the subset of crossimplices of the form $\{v_0^1, \ldots, v_k^1\} \subset V_1^{k+1}$, and $X_{-1,l}$ as the subset of crossimplices of the form $\{v_0^2, \ldots, v_l^2\} \subset V_2^{l+1}$. Such crossimplices will be referred to as *intralayer simplices* or *horizontal simplices*. We then obtain two simplicial complexes (Hatcher, 2000), $X_{\bullet,-1}$ and $X_{-1,\bullet}$, that we will refer to as the *intralayer complexes* and whose vertex sets are V_1 and V_2, respectively. In particular, $X_{1,-1}$ and $X_{-1,1}$ are graphs with vertex sets V_1 and V_2, respectively.

The *dimension* of a (k, l)-crossimplex is $k + l + 1$, and the dimension of CSB X is the dimension of its crossimplices of the highest dimension. The *n-skeleton* of X is the restriction of X to (k, l)-crossimplices such that $k + l + 1 \leq n$. In particular, the 1-skeleton of CSB is a two-layered network, with $X_{0,0}$ being the set of inter-layer

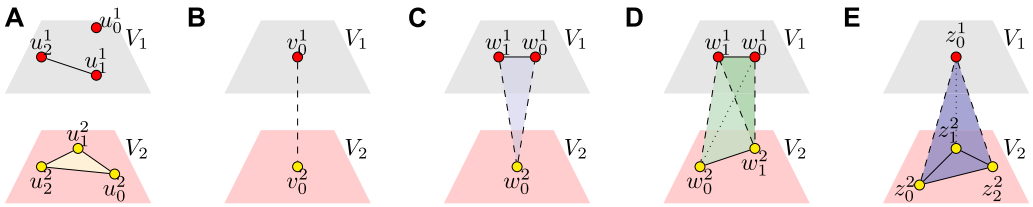

FIGURE 1
Crossimplices. Schematic representation of **(A)** A (0, −1)-crossimplex (a top vertex), a (1, −1)-crossimplex (top horizontal edge), and a (−1, 2)-crossimplex (bottom horizontal triangle); **(B)** (0,0)-crossimplex (a cross-edge); **(C)** (1,0)-crossimplex (a top cross-triangle); **(D)** (1,1)-crossimplex (a cross-tetrahedron); and **(E)** (0,2)-crossimplex (also a cross-tetrahedron). Notice that cross-edges are always oriented from the vertex of the top layer to that in the bottom layer. Therefore, cross-edges belonging to a cross-triangle are always of opposite orientations with respect to any orientation of the cross-triangle. There are two types of cross-triangles: the (1,0)-crossimplices (top cross-triangles) and (0,1)-crossimplices (bottom cross-triangle). Moreover, there are three types of cross-tetrahedrons: the (0,2)-crossimplices, (2,0)-crossimplices, and (1,1)-crossimplices.

links. Conversely, given a two-layered network Γ formed by two graphs $\Gamma_1 = (V_1, E_1)$ and $\Gamma_2 = (E_2, V_2)$ with the inter-layer edge set $E_{1,2} \subset V_1 \times V_2$, define a (k, l)-*clique* in Γ as a pair (σ_1, σ_2), where σ_1 is a k-clique in Γ_1 and σ_2 is an l-clique in Γ_2 with the property that $(i, j) \in E_{1,2}$ for every $i \in \sigma_1$ and $j \in \sigma_2$. We define the *cross-clique bicomplex* X associated with Γ by letting $X_{k,l}$ to be the set of all $(k + 1, l + 1)$-*cliques* in Γ.

Now, a *crossimplicial multicomplex* (CSM) $\mathcal{X}$ consists of a family of finite sets $V_s, s \in S \subseteq \mathbb{N}$ and a CSB $\mathcal{X}^{s,t}$ for each pair of distinct indices $s, t \in S$. It is *undirected* if the sets of crossimplices in $\mathcal{X}^{s,t}$ and $\mathcal{X}^{t,s}$ are in one-to-one correspondence. In such a case, $\mathcal{X}$ is completely defined by the family of CSB $\mathcal{X}^{s,t}$ with $s < t$ (see Figure 2 for a visualization of a three-layered CSM).

2.2 Orientation on crossimplices

The *orientation* of a (k, l)-crossimplex is an ordering choice over its vertices. When equipped with an orientation, the crossimplex is said to be *oriented* and will be represented as $[a] = [v_0^1, \ldots, v_k^1; v_0^2, \ldots, v_l^2]$ if $k, l \geq 0$, or $[v_0^1, \ldots, v_k^1]$ (resp. $[v_0^2, \ldots, v_l^2]$) if $k \geq 0$ and $l = -1$ (resp. $k = -1$ and $l \leq 0$). We shall note that an orientation of crossimplices is just a choice purely made for computational purposes. Extending geometric representations from simplicial complexes, crossimplices can be represented as geometric objects.

Specifically, a (0, −1)-crossimplex is a vertex in the top layer; a (0,0)-crossimplex is a *cross-edge* between layers V_1 and V_2; a (1, −1)-crossimplex (resp (−1, 1)-crossimplex) is a *horizontal edge* on V_1 (resp. V_2); a (0,1)-crossimplex or a (1,0)-crossimplex is a *cross-triangle*; a (2, −1)-crossimplex or (−1, 2)-crossimplex is a *horizontal triangle* on layer V_1 or V_2; a (3, −1)-crossimplex or (−1, 3)-crossimplex is a *horizontal tetrahedron* on V_1 or V_2; and a (1,1)-crossimplex, a (2,0)-crossimplex, or a (0,2)-crossimplex is a *cross-tetrahedron* (see Figure 1 for illustrations). On the other hand, *horizontal* edges, triangles, tetrahedrons, are just usual simplices on the horizontal complexes. One can consider a cross-edge as a connection between a vertex from one layer to a vertex on the other layer. In the same vein, a cross-triangle can be considered a connection between a vertex from one layer and two vertices on the other, and a cross-tetrahedron as a connection between either two vertices from one layer and two vertices on the other, or one vertex from one layer to three vertices on the other.

2.3 Weighted CSBs

A *weight* on CSB X is a positive function $w: \bigcup_{k,l} X_{k,l} \to \mathbb{R}^+$ that does not depend on the orientations of crossimplices. A *weighted CSB* is one that is endowed with a weight function. The *weight of a crossimplex* $a \in X$ is the number $w(a)$.

3 Topological descriptors

3.1 Cross-boundaries

CSB X defines a *bi-simplicial set* (Moerdijk, 1989; Goerss and Jardine, 2009) by considering, respectively, the *top* and *bottom crossface maps* $d^{(1)}_{i|k,l}: X_{k,l} \to X_{k-1,l}$ and $d^{(2)}_{i|k,l}: X_{k,l} \to X_{k,l-1}$ by

$$\begin{aligned} d^{(1)}_{i|k,l}([v_0^1, \ldots, v_k^1; v_0^2, \ldots, v_l^2]) &= [v_0^1, \ldots, \widehat{v_i^1}, \ldots, v_k^1; v_0^2, \ldots, v_l^2] \\ d^{(2)}_{i|k,l}([v_0^1, \ldots, v_k^1; v_0^2, \ldots, v_l^2]) &= [v_0^1, \ldots, v_k^1; v_0^2, \ldots, \widehat{v_i^2}, \ldots, v_k^2], \end{aligned} \quad (1)$$

where the hat over a vertex means dropping the vertex. Moreover, for a fixed $l \geq -1$, $X_{\bullet,l} = (X_{k,l})_{k \geq -1}$ is a simplicial complex. Similarly, $X_{k,\bullet} = (X_{k,l})_{l \geq -1}$ is a simplicial complex. We observe that if $a = \{v_0^1, \ldots, v_k^1, v_0^2, \ldots, v_l^2\} \in X_{k,l}$, then $a^{(1)} = \{v_0^1, \ldots, v_k^1\} \in X_{k,-1}$ and $a^{(2)} = \{v_0^2, \ldots, v_l^2\} \in X_{-1,l}$. We will refer to $a^{(1)}$ and $a^{(2)}$ as *the top horizontal face* and *the bottom horizontal face* of a, respectively. Conversely, two horizontal simplices, $v^1 \in X_{k,-1}$ and $v^2 \in X_{-1,l}$, are said to be *interconnected* in X if they are, respectively, the top and bottom horizontal faces of a (k, l)-crossimplex a. We then write $v^1 \sim v^2$. This is equivalent to requiring that if $v^1 = \{v_0^1, \ldots, v_k^1\}$ and $v^2 = \{v_0^2, \ldots, v_l^2\}$, then $\{v_0^1, \ldots, v_k^1, v_0^2, \ldots, v_l^2\} \in X_{k,l}$. If $a = \{v_0^1, \ldots, v_k^1, v_0^2, \ldots, v_l^2\} \in X_{k,l}$, we define its *top cross-boundary* $\partial^{(1)}a$ as the subset of $X_{k-1,l}$ consisting of all the top crossfaces of a, *i.e.*, all the $(k-1, l)$-crossimplices of the form $d^{(1)}_{i|k,l}[a]$ for $i = 0, \ldots, k$. Analogously, its *bottom cross-boundary* $\partial^{(2)}a \subseteq X_{k,l-1}$ is the subset of all its bottom crossfaces $d^{(2)}_{i|k,l}[a], \quad i = 0, \ldots, l$.

Now, two (k, l)-crossimplices $a, b \in X_{k,l}$ are said to be as follows:

- *top-outer (TO) adjacent*, which we write $a \frown^{(1)} b$ or $a \frown^{(1)}_c b$, if both are top crossfaces of a $(k + 1, l)$-crossimplex c; in other words, $a, b \in \partial^{(1)}c$;
- *top-inner (TI) adjacent*, which we write $a \smile_{(1)} b$ or $a \smile^d_{(1)} b$, if there exists a $(k - 1, l)$-crossimplex $d \in X_{k-1,l}$, which is a top crossface of both a and b, *i.e.*, $d \in \partial^{(1)}a \cap \partial^{(1)}_b$;

- *bottom-outer (BO) adjacent*, which we write $a \cap_b^{(2)}$ or $a \cap_c^{(2)} b$, if both are bottom crossfaces of a $(k, l+1)$-crossimplex $c \in X_{k,l+1}$; in other words, $a, b \in \partial^{(2)} c$; and
- *bottom-inner (BI) adjacent*, which we write $a \cup_{(2)} b$ or $a \cup_{(2)}^{d} b$, if there exists a $(k, l-1)$-crossimplex $f \in X_{k,l-1}$, which is a bottom face of both a and b; i.e., $d \in \partial^{(2)} a \cap \partial^{(2)} b$.

3.2 Degrees of crossimplices

Given a weight function w on X, we define the following degrees of a (k, l)-crossimplex a relative to w.

- The *TO degree* of a is the number:

$$\deg_{TO}(a) = \deg_{TO}(a, w) \coloneqq \sum_{\substack{a' \in X_{k+1,l} \\ a \in \partial^{(1)} a'}} w(a'). \tag{2}$$

- Similarly, the *TI degree* of a is defined as follows:

$$\deg_{TI}(a) = \deg_{TI}(a, w) \coloneqq \sum_{\substack{c \in X_{k-1,l} \\ c \in \partial^{(1)} a}} \frac{1}{w(c)}. \tag{3}$$

- Analogously, the *BO degree* of a is given as follows:

$$\deg_{BO}(a) = \deg_{BO}(a, w) \coloneqq \sum_{\substack{a' \in X_{k,l+1} \\ a \in \partial^{(2)} a'}} w(a'). \tag{4}$$

- The *BO degree* of a is as follows:

$$\deg_{BI}(a) = \deg_{BI}(a, w) \coloneqq \sum_{\substack{c \in X_{k,l-1} \\ c \in \partial^{(2)} a}} \frac{1}{w(c)}. \tag{5}$$

Observe that in the particular case where the weight function is equal to one everywhere, the TO degree of a is precisely the number of $(k+1, l)$-crossimplices in X, of which a is the top crossface, while $\deg_{TI}(a)$ is the number of top crossfaces of a, which equals to $k+1$. Analogous observations can be made about the BO and BI degrees.

3.3 Cross-homology groups

The space $C_{k,l}$ of (k, l)-*cross-chains* is defined as the real vector space generated by all oriented (k, l)-crossimplexes in $\mathcal{X}$. The *top* and *bottom cross-boundary operators* $\partial_{k,l}^{(1)} \colon C_{k,l} \to C_{k-1,l}$ and $\partial_{k,l}^{(2)} \colon C_{k,l} \to C_{k,l-1}$ are then defined as follows by the formula

$$\partial_{k,l}^{(s)}([a]) \coloneqq \sum_{b \in \partial^{(s)} a} \operatorname{sgn}\left(b, \partial^{(s)} a\right)[b], \tag{6}$$

for $s = 1, 2$ and a generator $a \in X_{k,l}$, where $\operatorname{sgn}(b, \partial^{(s)} a)$ is the sign of the orientation of b in $\partial^{(s)} a$; in other words, if $b = d_{i|k,l}^{(1)}[a]$, then $\operatorname{sgn}(b, \partial^{(1)} a) \coloneqq (-1)^i$, and we define $\operatorname{sgn}(b, \partial^{(2)} a)$ in a similar fashion.

It is straightforward to see that in particular

$$\partial_{k,-1}^{(1)} \colon C_{k,-1} \to C_{k-1,-1}, k \geq 0$$

and

$$\partial_{-1,l}^{(2)} \colon C_{-1,l} \to C_{-1,l}, l \geq 0$$

are the usual boundary maps of simplicial complexes. For this reason, we focus more on the mixed case where both l and k are non-negative. We will often drop the indices and write $\partial^{(1)}$ and $\partial^{(2)}$ to avoid cumbersome notations. To see how these maps operate, let us compute, for instance, the images of the crossimplices (b), (c), (d), and (e) illustrated in Figure 1. We obtain the following:

$$\begin{cases} \partial_{0,0}^{(1)}[v_0^1; v_0^2] = [v_0^2] \in C_{-1,0} \\ \partial_{0,0}^{(2)}[v_0^1; v_0^2] = -[v_0^1] \in C_{0,-1}; \end{cases}$$

$$\begin{cases} \partial_{1,0}^{(1)}[w_0^1, w_1^1; w_0^2] = [w_1^1; w_0^2] - [w_0^1; w_0^2] \in C_{0,0}, \\ \partial_{1,0}^{(2)}[w_0^1, w_1^1; w_0^2] = [w_0^1, w_1^1] \in C_{1,-1}; \end{cases}$$

$$\begin{cases} \partial_{1,1}^{(1)}[w_0^1, w_1^1; w_0^2, w_1^2] = [w_1^1; w_0^2, w_1^2] - [w_0^1; w_0^2, w_0^2] \in C_{0,1}, \\ \partial_{1,1}^{(2)}[w_0^1, w_1^1; w_0^2, w_1^2] = [w_0^1, w_1^1; w_1^2] - [w_0^1, w_1^1; w_0^2] \in C_{1,0}; \end{cases}$$

$$\begin{cases} \partial_{0,2}^{(1)}[z_0^1; z_0^2, z_1^2, z_2^2] = [z_0^2, z_1^2, z_2^2] \in C_{-1,2} \\ \partial_{0,2}^{(2)}[z_0^1; z_0^2, z_1^2, z_2^2] = [z_0^1; z_1^2, z_2^2] - [z_0^1; z_0^2, z_2^2] \\ \qquad\qquad + [z_0^1; z_0^2, z_1^2] \in C_{0,1}. \end{cases}$$

Notice that $\partial_{0,-1}^{(1)} = \partial_{-1,0}^{(2)} = 0$. Moreover, by simple calculations from (6), it is easy to check that $\partial_{k-1,l}^{(1)} \partial_{k,l}^{(1)} = 0$ and $\partial_{k,l-1}^{(2)} \partial_{k,l}^{(2)} = 0$, which allows to define the *top* and *bottom* (k, l)-*cross-homology groups* of X as the following quotients:

$$\mathrm{H}_{k,l}^{(1)}(X) \coloneqq \ker \partial_{k,l}^{(1)} \big/ \operatorname{im} \partial_{k+1,l}^{(1)}, \text{ and}$$

$$\mathrm{H}_{k,l}^{(2)}(X) \coloneqq \ker \partial_{k,l}^{(2)} \big/ \operatorname{im} \partial_{k,l+1}^{(2)}.$$

For $k \geq 0$ and $l \leq 0$, $\partial_{k,-1}^{(1)}$ and $\partial_{-1,l}^{(2)}$ are the usual boundary maps of simplicial complexes (Hatcher, 2000). Therefore, $\mathrm{H}_{k,-1}^{(1)}(X)$ and $\mathrm{H}_{-1,l}^{(2)}(X)$ are the usual homology groups (Mac Lane, 1963; Hatcher, 2000) of the simplicial complexes $X_{\bullet,-1}$ and $X_{-1,\bullet}$, respectively.

3.4 Cross-Betti vectors

The cross-homology groups are completely determined by their dimensions, the *top* and *bottom* (k, l)-*cross-Betti numbers* $\beta_{k,l}^{(s)}(X) = \dim \mathrm{H}_{k,l}^{(s)}(X)$, $s = 1, 2$. In particular, $\beta_{k,-1}^{(1)}$ and $\beta_{-1,l}^{(2)}$ are the usual Betti numbers for the horizontal simplicial complexes (Hatcher, 2000). The couple $\beta_{k,l} = (\beta_{k,l}^{(1)}, \beta_{k,l}^{(2)})$ is the (k, l)-*cross-Betti vector* of X and can be computed using basic linear algebra. These vectors are descriptors of the topologies of both the horizontal complexes and their inter-connections. For instance, $\beta_{0,-1}$ and $\beta_{-1,0}$ encode the connectivities within and in-between the 1-skeletons of the horizontal complexes associated with X. Precisely, $\beta_{0,-1}^{(1)}$ is the number of connected components of the graph $X_{1,-1}$, and $\beta_{0,-1}^{(2)}$ is the number of nodes in V_1 with no interconnections with any nodes in V_2. Similarly, $\beta_{-1,0}^{(1)}$ is the number of nodes in V_2 with no interconnections with any nodes in V_1, while $\beta_{-1,0}^{(2)}$ is the number of connected components of the bottom horizontal graph $X_{-1,1}$. Furthermore, $\beta_{1,-1}$ simultaneously counts the number of loops in $X_{1,-1}$ and the number of its intra-layer links that do not belong to

10.3389/fcpxs.2023.1281714

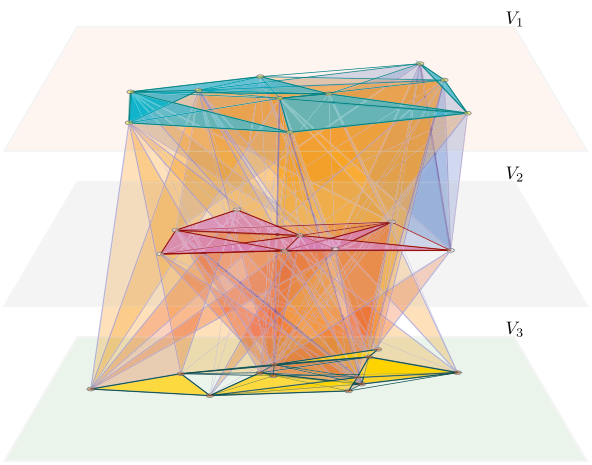

FIGURE 2
Schematic representation of a two-dimensional crossimplicial multicomplex $\mathcal{X}$ with 3 layers and 30 nodes in total; $\mathcal{X}$ consists of the vertex sets V_1, V_2, and V_3 and the three CSBs $\mathcal{X}^{1,2}, \mathcal{X}^{1,3}, \mathcal{X}^{2,3}$ defined, respectively, on the products $V_1 \times V_2$, $V_1 \times V_3$, and $V_2 \times V_3$.

TABLE 1 Cross-Betti table. The cross-Betti table for CSM of Figure 2. The table quantifies the connectedness of the three horizontal complexes, the number of cycles in each of them, the number of nodes in each layer that are not connected to the other layers, the number of intra-layer edges not belonging to any cross-triangles, and the number of paths of length 2 connecting the nodes in one layer and passing through a node from another layer.

	$\mathcal{X}^{1,2}$	$\mathcal{X}^{1,3}$	$\mathcal{X}^{2,3}$
$\beta^{\otimes}_{0,-1}$	(1,0)	(1,0)	(1,0)
$\beta^{\otimes}_{1,-1}$	(13,21)	(13,21)	(6,14)
$\beta^{\otimes}_{-1,0}$	(0,1)	(1,1)	(0,1)
$\beta^{\otimes}_{-1,1}$	(17,6)	(29,16)	(29,16)
$\beta^{\otimes}_{0,0}$	(11,14)	(20,24)	(19,23)

cross-triangles formed with the graph $X_{-1,1}$. Analogous topological information is provided by $\beta_{-1,1}$. In addition, $\beta_{0,0}$ measures the extent to which individual nodes of one complex layer serve as communication channels between different hubs from the other layers. More precisely, an element in $\mathrm{H}^{(1)}_{0,0}(X)$ represents either an inter-layer one-dimensional loop formed by a path in $X_{1,-1}$, whose end-nodes interconnect with the same node in V_2, or two connected components in the top complex communicating with each other through a node in the bottom complex. $\beta_{0,0}$ counts the shortest paths of length 2 between nodes within one layer passing through a node from the other layer and not belonging to the cross-boundaries of cross-triangles; we call such paths *cones*. In other words, $\beta_{0,0}$ quantifies node clusters in one layer that are "controlled" by nodes in the other layer. Detailed proof of this description is provided in Methods 7.1.

Now, given a CSM $\mathcal{X}$, its *cross-Betti table* $\beta^{\otimes}_{k,l}$ is obtained by computing all the cross-Betti vectors of all its underlying CSBs. Computation of the cross-Betti table of the CSM of Figure 2 is presented in Table 1.

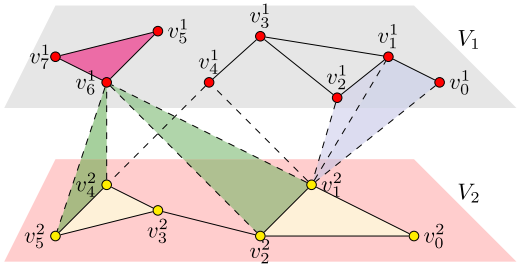

FIGURE 3
Cross-Betti vectors. Schematic representation of a two-dimensional CSB with 14 nodes in total, whose oriented maximal crossimplices are the intra-layer triangle $[v^1_5, v^1_6, v^1_7]$ in $X_{2,-1}$, the intra-layer edges $[v^1_0, v^1_1]$, $[v^1_1, v^1_2]$, $[v^1_1, v^1_3]$, $[v^1_2, v^1_3]$ in $X_{1,-1}$, the bottom intra-layer triangles $[v^2_0, v^2_1, v^2_2]$, $[v^2_3, v^2_4, v^2_5]$ in $X_{-1,2}$, the intra-layer edge $[v^2_2, v^2_3]$ in $X_{-1,1}$, the cross-triangles $[v^1_0, v^1_1; v^2_1]$, $[v^1_1, v^1_2; v^2_1]$ in $X_{1,0}$, $[v^1_6; v^2_1, v^2_2]$, $[v^1_6; v^2_4, v^2_5]$ in $X_{0,1}$, and the cross-edges $[v^1_4; v^2_1]$, $[v^1_4; v^2_4]$ in $X_{0,0}$.

To illustrate what the cross-Betti vectors represent, we consider the simple two-dimensional CSB X of Figure 3. We get $\beta^{(1)}_{0,-1} = 2, \beta^{(1)}_{1,-1} = 1$ and $\beta^{(2)}_{-1,0} = 1, \beta^{(2)}_{-1,1} = 0$. This reflects the fact the top layer has two connected components and one cycle, while the bottom one has one component and no cycles. Moreover, three top nodes are not interconnected to the bottom complex, six top edges are not top faces of cross-triangles, two bottom nodes are not interconnected to the top layer, and five bottom edges are not bottom faces of cross-triangles. This information is encoded in $\beta_{0,-1} = (2, 3)$, $\beta_{1,-1} = (1, 6)$, $\beta_{-1,0} = (2, 1)$, and $\beta_{-1,1} = (5, 0)$. There are three generating inter-layer cycles, two of which are formed by an intra-layer path in the bottom layer and a node in the top layer (v^1_4 and v^1_6), and the other one is formed by an intra-layer path in the top layer and a node (v^2_1) in the bottom layer. Moreover, the two nodes v^2_1 and v^2_4 of V_2 interconnect the two separated components of the top layer; they serve as *cross-hubs*: removing both nodes eliminates all communications between the two components of the top layer. Cross-hubs and these types of inter-layer cycles are exactly what $\beta_{0,0}$ encodes. Specifically, by computing the cross-homology of X, we get $\beta^{(1)}_{0,0} = 3$, which counts the cycle $v^1_2 - v^1_3 - v^1_4 - v^2_1 - v^1_2$ and the nodes v^2_4 and v^2_1 that interconnect v^1_4 to v^1_6, and v^1_2 to v^1_6, $\beta^{(2)}_{0,0} = 2$ counting the inter-layer cycles $v^1_4 - v^2_1 - v^2_2 - v^2_3 - v^2_4 - v^1_4$ and $v^1_6 - v^2_2 - v^2_3 - v^2_4 - v^1_6$. In each of these cycles, the top node allows a shortest (inter-layer) path between the end-points of the involved intra-layer path.

Using algebraic topological methods to calculate the cross-Betti vectors for larger multicomplexes can quickly become computationally heavy. We provide powerful linear-algebraic tools that not only allow to easily compute $\beta_{k,l}$s but also tell exactly where the topological structures being counted are located within the multicomplex.

4 Spectral descriptors

4.1 Cross-forms

$C^{k,l} := C^{k,l}(X, \mathbb{R})$ denotes the dual space $\mathrm{Hom}_{\mathbb{R}}(C_{k,l}, \mathbb{R})$ of the real vector space $C_{k,l}$. In other words, $C^{k,l}$ is the vector space of real

linear functional ϕ: $C_{k,l} \to \mathbb{R}$. We will refer to such functionals as (k, l)-*forms* or *cross-forms* on X. In particular, (k, −1)-forms correspond to k-forms on the simplicial complex $X_{\bullet,-1}$, and (−1, l)-forms are l-forms on the complex $X_{-1,\bullet}$. We have $C^{-1,-1} = 0$, and by convention, we set $C^{k,l}(\varnothing) = 0$.

Notice that a natural basis of $C^{k,l}$ is given by the following set of linear forms:

$$\{e_a \colon C_{k,l} \to \mathbb{R},\ a \in X_{k,l}\},$$

called *elementary cross-forms*, where

$$e_a(b) = \begin{cases} 1, & \text{if } a = b, \\ 0, & \text{otherwise,} \end{cases}$$

which naturally identify $C^{k,l}$ with $C_{k,l}$. Now, the maps $\delta^{(1)}_{k,l} \colon C^{k,l} \to C^{k+1,l}$ and $\delta^{(2)}_{k,l} \colon C^{k,l} \to C^{k,l+1}$ are defined by the following equations:

$$\begin{aligned} \delta^{(1)}_{k,l}\phi([a]) &= \sum_{b \in \partial^{(1)} a} \operatorname{sgn}\left(b, \partial^{(1)} a\right)\phi([b]), \\ \delta^{(2)}_{k,l}\phi([c]) &= \sum_{d \in \partial^{(2)} c} \operatorname{sgn}\left(d, \partial^{(2)} c\right)\phi([d]), \end{aligned} \tag{7}$$

for $\phi \in C^{k,l}$, $a \in X_{k+1,l}$ and $c \in X_{k,l+1}$. Next, given a weight w on X, we get an inner product on cross-forms by the following setting:

$$\langle \phi, \psi \rangle_{k,l} \coloneqq \sum_{a \in X_{k,l}} w(a)\phi(a)\psi(a), \text{ for } \phi, \psi \in C^{k,l}. \tag{8}$$

It can been seen that, with respect to this inner product, elementary cross-forms form an orthogonal basis, and by simple calculations, the dual maps are given by the following equation:

$$\left(\delta^{(1)}_{k,l}\right)^* \phi([a]) = \sum_{\substack{a' \in X_{k+1,l} \\ a \in \partial^{(1)} a'}} \frac{w(a')}{w(a)} \operatorname{sgn}\left(a, \partial^{(1)} a'\right)\phi([a']), \tag{9}$$

for $\phi \in C^{k+1,l}$, $a \in X_{k,l}$. We also obtain a similar formula for the dual $(\delta^{(2)}_{k,l})^*$.

4.2 The cross-Laplacian operators

Identifying $C_{k,l}$ with $C^{k,l}$ and equipping it with an inner product, as (21), we define the following self-adjoint linear operators on $C_{k,l}$ for all k, $l \geq -1$:

- the *top* (k, l)-*cross-Laplacian* is as follows:

$$\mathcal{L}^{(\mathrm{T})}_{k,l} \coloneqq \left(\delta^{(1)}_{k,l}\right)^* \delta^{(1)}_{k,l} + \delta^{(1)}_{k-1,l}\left(\delta^{(1)}_{k-1,l}\right)^*;$$

- and the *bottom* (k, l)-*cross-Laplacian* is as follows:

$$\mathcal{L}^{(\mathrm{B})}_{k,l} \coloneqq \left(\delta^{(2)}_{k,l}\right)^* \delta^{(2)}_{k,l} + \delta^{(2)}_{k,l-1}\left(\delta^{(2)}_{k,l-1}\right)^*.$$

Being defined on finite dimensional spaces, these operators can be represented as square matrices indexed over crossimplices. Specifically, denoting $N_{k,l} = |X_{k,l}|$, $\mathcal{L}^{(\mathrm{T})}_{k,l}$ can be represented by positive definite $N_{k,l} \times N_{k,l}$ matrices (see Methods 7.3).

Moreover, the null spaces, the elements of which we call *harmonic cross-forms*, are easily seen to be in one-to-one correspondence with cross-cycles on X. In other words, we have the following isomorphisms (see Methods 7.2 for the proof):

$$\mathrm{H}^{(1)}_{k,l}(X) \cong \ker \mathcal{L}^{(\mathrm{T})}_{k,l},\ \mathrm{H}^{(2)}_{k,l}(X) \cong \ker \mathcal{L}^{(\mathrm{B})}_{k,l}.$$

It follows that in order to compute the cross-Betti vectors, it suffices to determine the dimensions of the eigenspaces of the zero-eigenvalues of the cross-Laplacians.

It should be noted that in addition to being much easier to implement, the spectral method to compute cross-homology has the advantage of providing a geometric representation of the cross-Betti numbers through eigenvectors. However, before we see how this works, let us make a few observations. Notice that $\mathcal{L}^{(\mathrm{T})}_{0,-1}$ and $\mathcal{L}^{(\mathrm{B})}_{-1,0}$ are the usual graph Laplacians of 0 degree for the horizontal complexes. More generally, $\mathcal{L}^{(\mathrm{T})}_{k,-1}$ and $\mathcal{L}^{(\mathrm{B})}_{-1,l}$ are the combinatorial higher Hodge Laplacians (Horak and Jost, 2013; Lim, 2020; Schaub et al., 2020) of degrees k and l, respectively, for the horizontal simplicial complexes. Furthermore, $\mathcal{L}^{(\mathrm{B})}_{k,-1}$ (resp. $\mathcal{L}^{(\mathrm{T})}_{-1,l}$) detects the k-simplices (resp. l-simplices) in the top (resp. bottom) layer complex that are not top (resp. bottom) faces of (k, 0)-crossimplices (resp. (0, l)-crossimplices). Moreover, one can see that $\mathcal{L}^{(\mathrm{B})}_{k,-1}$ is the diagonal matrix indexed over the k-simplices on the top complex and whose diagonal entries are the BO degrees. Similarly, $\mathcal{L}^{(\mathrm{T})}_{-1,l}$ is the diagonal matrix whose diagonal entries are the TO degrees of the l-simplices on the bottom complex. This is consistent with the interpretation of the cross-Betti numbers $\beta^{(2)}_{0,-1}$ and $\beta^{(1)}_{-1,0}$ given earlier in terms of connectivities between the 1-skeletons of the horizontal complexes.

TABLE 2 Harmonic (0,0) cross-forms. The three eigenvectors of the eigenvalue 0 of $\mathcal{L}^{(\mathrm{T})}_{0,0}$ corresponding to the synthetic CSB of Figure 3. There are two harmonic cross-hubs, v^2_1 and v^2_4, and their respective harmonic cross-hubness are 2.6177 and 1.4070.

ω_1	ω_2	ω_3	
0.0290	−0.2872	0.2236	$[v^1_0; v^2_1]$
0.0290	−0.2872	0.2236	$[v^1_1; v^2_1]$
0.0290	−0.28721	0.2236	$[v^1_2; v^2_1]$
0.0	0.0	−0.8944	$[v^1_4; v^2_1]$
0.7035	0.0710	0.0	$[v^1_4; v^2_4]$
−0.0870	0.8616	0.2236	$[v^1_6; v^2_1]$
0.0	0.0	0.0	$[v^1_6; v^2_2]$
−0.7035	−0.0710	0.0	$[v^1_6; v^2_4]$
0.0	0.0	0.0	$[v^1_6; v^2_5]$

4.3 Harmonic cross-hubs

For the sake of simplicity, it is assumed that X is equipped with the trivial weight ≅1. Then, by (26), the (0,0) cross-Laplacians $\mathcal{L}^{(\mathrm{T})}_{0,0}$ and $\mathcal{L}^{(\mathrm{B})}_{0,0}$ are, respectively, represented by the $N_{0,0} \times N_{0,0}$ matrices indexed on cross-edges a_i, $a_j \in X_{0,0}$, whose entries are given by the following equations:

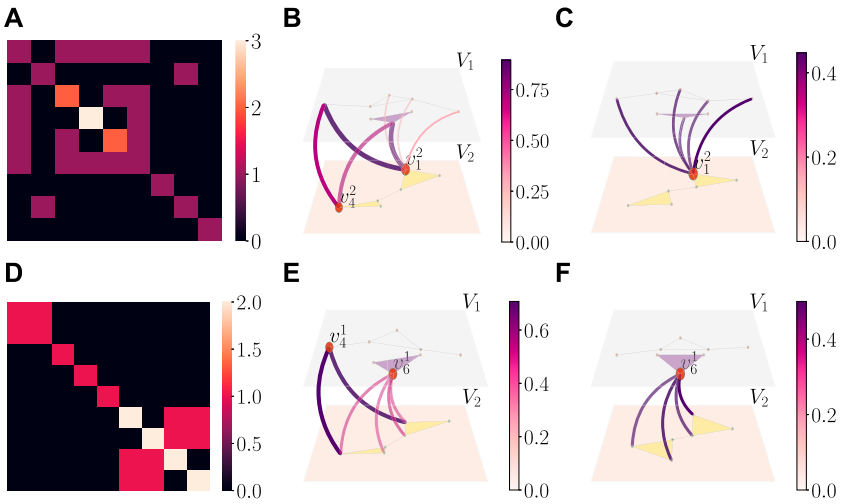

FIGURE 4
Cross-Laplacians, harmonic, and principal cross-hubs. **(A)** and **(D)** Heat-maps of the top and bottom (0,0) cross-Laplacian matrices for the example in Figure 3. Both matrices are indexed over the cross-edges of CSB, and the diagonal entries correspond to one added to the number of cross-triangles containing the corresponding cross-edge. $\mathcal{L}_{0,0}^{(\mathrm{T})}$ has a zero eigenvalue of multiplicity 3, while $\mathcal{L}_{0,0}^{(\mathrm{B})}$ has a zero eigenvalue of multiplicity 2. **(B)** and **(E)** Harmonic cross-hubs with respect to the top (resp. the bottom) horizontal complex of X; the *intensity* of a cross-edge is given by the L^1-norm of the corresponding coordinates in the eigenvectors of the eigenvalue 0. **(C)** and **(F)** *Principal cross-hubs* in the bottom (resp. top) layer with respect to the top (resp. bottom) layer; by definition, they are the spectral cross-hubs obtained from the largest eigenvalues of the top and bottom (0,0) cross-Laplacians, respectively.

$$\left(\mathcal{L}_{0,0}^{(\mathrm{T})}\right)_{a_i,a_j} = \begin{cases} \deg_{TO}(a_i) + 1, & \text{if } i = j, \\ 1, & \text{if } i \neq j,\ [a_i] = \left[v_i^1; v_k^2\right], \\ & \left[a_j\right] = \left[v_j^1; v_k^2\right] \\ & \text{and } \left\{v_i^1, v_j^1, v_k^2\right\} \notin X_{1,0}, \\ 0, & \text{otherwise,} \end{cases} \tag{10}$$

and

$$\left(\mathcal{L}_{0,0}^{(\mathrm{B})}\right)_{a_i,a_j} = \begin{cases} \deg_{BO}(a_i) + 1, & \text{if } i = j, \\ 1, & \text{if } [a_i] = \left[v_{i_0}^1; v_i^2\right], \\ & \left[a_j\right] = \left[v_{i_0}^1; v_j^2\right], \\ & \text{and } \left\{v_{i_0}^1, v_i^2, v_j^2\right\} \notin X_{0,1}, \\ 0, & \text{otherwise.} \end{cases} \tag{11}$$

Applied to the toy example of Figure 3, $\mathcal{L}_{0,0}^{(\mathrm{T})}$ has a zero-eigenvalue of multiplicity 3, generating the three (0,0) cross-cycles in Table 2.

Each coordinate in the eigenvectors is seen as an "intensity" along the corresponding cross-edge. Cross-edges with non-zero intensities sharing the same bottom node define certain communities in the top complex that are "controlled" by the involved bottom node. These community structures depend on both the underlying topology of the top complex and its interdependence with the other complex layer. We then refer to them as *harmonic cross-clusters*, and the bottom nodes controlling them are considered *harmonic cross-hubs* (HCHs). The *harmonic cross-hubness* of a bottom node is the L^1-norm of the intensities of all cross-edges having it in common. Here, in the eigenvectors of the eigenvalue 0, there are two subsets of cross-edges with non-zero coordinates: the cross-edges with v_1^2 in common and those with v_4^2 in common. We, therefore, have two harmonic cross-hubs (see illustration in Figure 4), hence two harmonic cross-clusters. The first harmonic cross-hub is responsible for the top layer cross-cluster $\{v_0^1, v_1^1, v_2^1, v_4^1, v_6^1\}$, while the second harmonic cross-hub controls the top layer cross-cluster $\{v_4^1, v_6^1\}$. The intensity of each involved cross-edge is the L^1-norm of its corresponding coordinates in the three eigenvectors, and the harmonic cross-hubness is the sum of the intensities of the cross-edges interconnecting the corresponding cross-hub to each of the top nodes in the cross-clusters it controls. For instance, v_1^2 is the bottom node with the highest harmonic cross-hubness, which is 2.6177. This reflects the fact that v_1^2 not only interconnects the two connected components of the top complex (which v_4^2 does as well) but it also allows fast-track connections between the highest number of nodes that are not directly connected with intra-layer edges in the top complex. The same calculations applied to the eigenvectors of the zero-eigenvalues of $\mathcal{L}_{0,0}^{(\mathrm{B})}$ yield v_6^1 as the top node with the highest harmonic cross-hubness with respect to the bottom complex.

4.4 Spectral persistence of cross-hubs

To better grasp the idea of cross-hubness, let us have a closer look at the coordinates of the eigenvectors of the (0,0) cross-Laplacians ((10) and (11)) whose eigenvalues are all non-negative real numbers. Suppose $\phi = (x_1, \ldots, x_{N_{0,0}})$ is an eigenvector for an eigenvalue λ^T of $\mathcal{L}_{0,0}^{(\mathrm{T})}$. Then, denoting the cross-edges by a_i, $i = 1, \ldots, N_{0,0}$, we have the following relations:

$$x_i = \frac{1}{\lambda^T - \deg_{TO}(a_i)} \sum_j \chi\left(a_i, a_j\right) x_j, \tag{12}$$

where χ is such that $\chi(a_i, a_j) = 1$ if $i = j$ or if a_i and a_j are adjacent but do not belong to a top cross-triangle, and $\chi(a_i, a_j) = 0$ otherwise. It follows that the cross-edge intensity $|x_i|$ grows larger as $\deg_{TO}(a_i) \rightarrow$

10.3389/fcpxs.2023.1281714

TABLE 3 Principal eigenvector of $\mathcal{L}^{(T)}_{0,0}$ for the CSB of Figure 3. By definition, this is the eigenvector associated with the largest eigenvalue.

0.4472	$[v_0^1; v_1^2]$
0.4472	$[v_1^1; v_1^2]$
0.4472	$[v_2^1; v_1^2]$
0.4472	$[v_4^1; v_1^2]$
0.0	$[v_4^1; v_4^2]$
0.4472	$[v_6^1; v_1^2]$
0.0	$[v_6^1; v_2^2]$
0.0	$[v_6^1; v_4^2]$
0.0	$[v_6^1; v_5^2]$

λ^T. In particular, for $\lambda^T = 0$, the intensity is larger for cross-edges that belong to a large number of cones and to the smallest number of top cross-triangles. Now, consider the other extreme of the spectrum, namely, $\lambda^T = \lambda^T_{\max}$, to be the largest eigenvalue of $\mathcal{L}^{(T)}_{0,0}$. Then, the intensity $|x_i|$ is larger for cross-edges belonging to the largest number of top cross-triangles and a large number of top cones at the same time.

Taking the case of a two-layered network, for $\lambda^T = 0$, $|x_i|$ is larger for a cross-edge pointing to a bottom node interconnecting the largest number of top nodes that are not directly connected with intra-layer edges; for $\lambda^T = \lambda_{\max}$, $|x_i|$ is larger for a cross-edge pointing to a bottom node interconnecting a large number of top intra-layer communities both with each other and with a large number of top nodes that are not directly connected to each other via intra-layer edges.

More generally, applying the same process to each distinct eigenvalue, we obtain clustering structures in the top layer that are *controlled* by the bottom nodes and that vary along the spectrum $\lambda^T_1 \leq \lambda^T_2 \leq \cdots \leq \lambda^T_{\max}$ of $\mathcal{L}^{(T)}_{0,0}$. At every stage, we regroup the cross-edges with non-zero coordinates in the associated eigenvectors and pointing to the same nodes, and then sum up their respective intensities to obtain a ranking among a number of cross-hubs that we call *spectral cross-hubs* (SCHs). Intuitively, the intensities held by cross-edges gather to confer a 'restructuring power' onto the common bottom node, the cross-hub, allowing it to control a cluster on the top layer. It is clear that, by permuting the top layer with the bottom layer, the same reasoning applies to $\mathcal{L}^{(B)}_{0,0}$. In particular, we define the *principal cross-hubs* (PCHs) in the bottom layer with respect to the top layer as the SCHs obtained from $\lambda^T_{\max}$. The *principal cross-hubness* of a bottom PCH is defined as its restructuring power. In a similar fashion, we define the principal cross-hubness in the top layer with respect to the bottom layer using the largest eigenvalue $\lambda^B_{\max}$ of $\mathcal{L}^{(B)}_{0,0}$. Going back to the bicomplex of Figure 3, the largest eigenvalue of $\mathcal{L}^{(T)}_{0,0}$ is $\lambda^T_{\max} = 5$, and the corresponding eigenvector is represented by Table 3.

There is only one PCH in the bottom layer with respect to the top layer, which is the bottom node v_1^2, and its principal cross-hubness is 2.2360.

Interestingly, the number of SCHs that appear for a given eigenvalue tend to vary dramatically with respect to the smallest eigenvalues before it eventually decreases or stabilizes at a very low number (see Figure 5; Figure 6). Some cross-hubs may appear at one stage along the spectrum and then disappear at a future stage. This suggests the notion of *spectral persistence* of cross-hubs. Nodes that emerge the most often or live longer as cross-hubs along the spectrum might be seen as the most central in restructuring the topology of the other complex layers. The further we move away from the smallest non-zero eigenvalue, the more powerful are the nodes that emerge as hubs facilitating communications between aggregations of nodes in the other layer. The emergence of spectral cross-hubs is represented by a horizontal line—*spectral persistence bar*—running through the indices of the corresponding eigenvalues (Figure 5). The spectral persistence bars corresponding to all SCHs (the *spectral bar codes*) obtained from $\mathcal{L}^{(T)}_{0,0}$ (resp. $\mathcal{L}^{(B)}_{0,0}$) constitute a *signature* for all the clustering structures imposed by the bottom (resp. top) layer to the top (resp. bottom) layer.

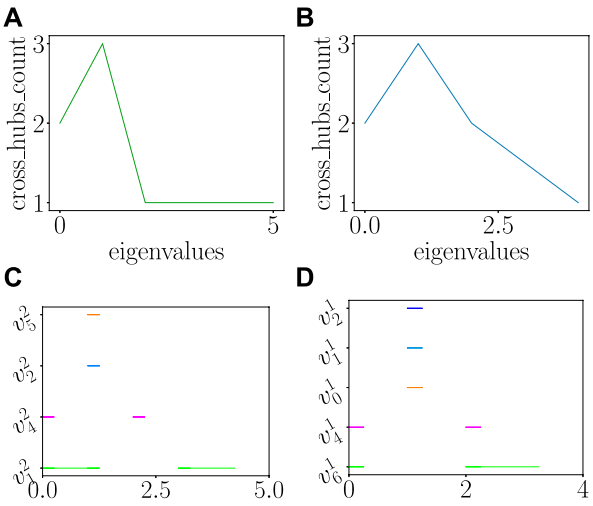

FIGURE 5
Spectral persistence of cross-hubs. Schematic illustrations of the variations in spectral cross-hubs along the eigenvalues and the spectral persistence bars codes for the toy CSB of Figure 3: **(A)** shows the number of bottom nodes that emerge as spectral cross-hubs with respect to the top layer as a function of the eigenvalues of $\mathcal{L}^{(T)}_{0,0}$, and **(B)** represents the number of top nodes revealed as spectral cross-hubs with respect to the bottom layer as a function of the eigenvalues of $\mathcal{L}^{(B)}_{0,0}$. **(C)** and **(D)** represent the *spectral persistence bar codes* for $\mathcal{L}^{(T)}_{0,0}$ and $\mathcal{L}^{(B)}_{0,0}$, respectively. For both the top and bottom (0,0) cross-Laplacians, most of the spectral cross-hubs, hence, spectral cross-clusters, emerge during the first stages (smallest eigenvalues), and very few of them survive at later stages; here, only one cross-hub emerges or survives at the largest eigenvalue (v_1^2 for $\mathcal{L}^{(T)}_{0,0}$ and v_6^1 for $\mathcal{L}^{(B)}_{0,0}$).

5 Experiments on multiplex networks

5.1 Diffusion CSBs

Let $\mathcal{M}$ be a multiplex formed by M graphs $\Gamma^s = (E_s, V)$, $s = 1, \ldots, M$. Denoting the vertex set V as an ordered set $\{1, 2, \ldots, N\}$, we will write v_i^s to represent the node i in the graph Γ^s, following the same notations we have used for multicomplexes.

For every pair of distinct indices s, t, we define the two-dimensional CSB $X^{s\to t}$ on $V \times V$ such that $X^{s\to t}_{k,-1} = \varnothing$ for $k \geq 1$,

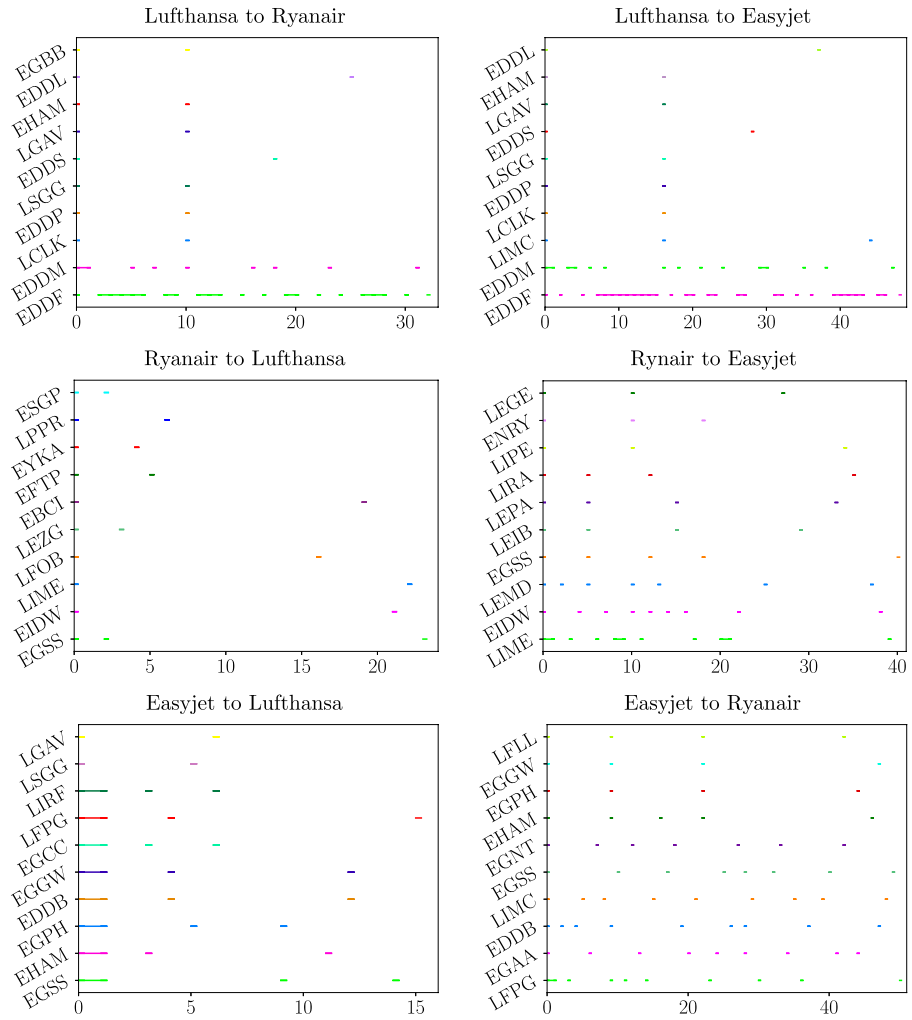

FIGURE 6
Spectral persistent cross-hubs. The spectral persistence bar codes of the six diffusion bicomplexes of the European ATN multiplex. The nodes represent European airports labeled with their ICAO codes (see https://en.wikipedia.org/wiki/ICAO_airport_code). The most persistent cross-hubs correspond to the airports that provide the most efficient correspondences from the first airline network to the second.

and $X^{s\to t}_{-1,k}$ is the 2-clique complex of the layer indexed by t in the multiplex $\mathcal{M}$; a pair $(v^s_i, v^t_j) \in V \times V$, forms a cross-edge if $i < j$, and nodes i and j are connected in Γ^s; and a (0,1) crossimplex is a triple $(v^s_i, v^t_j, v^t_k) \in V^3$ such that i is connected to j and k in Γ^s, and j and k are connected in Γ^t, while $X^{s\to t}_{1,0} = \varnothing$. We call $X^{s\to t}$ the *diffusion bicomplex* of (layer) s onto t. Notice that by construction, the (0,0) cross-Laplacians of $X^{s\to t}$ are indexed over E_s, while the (0,0) cross-Laplacians of $X^{t\to s}$ are indexed over E_t. This shows that $X^{s\to t}$ and $X^{t\to s}$ are not the same. The diffusion bicomplex $X^{s\to t}$ is a way to look at the topology of Γ^s through the topology of Γ^t; in other words, it diffuses the topology of the former into the topology of the latter.

5.2 Cross-hubs in air transportation networks

We used a subset of the European air transportation network (ATN) dataset (from Cardillo et al., 2013) to construct a three-layered multiplex $\mathcal{M}$ on 450 nodes, each representing a European airport (Wu et al., 2019). The three layer networks Γ^1, Γ^2, and Γ^3 of $\mathcal{M}$ represent the direct flights served by Lufthansa, Ryanair, and easyJet airlines, respectively, that is, intra-layer edges correspond to direct flights between airports served by the corresponding airline. Considering the respective bottom (0,0) cross-Laplacians of the six diffusion bicomplexes $X^{1\to 2}$, $X^{1\to 3}$, $X^{2\to 1}$, $X^{3\to 1}$, $X^{2\to 3}$, and $X^{3\to 2}$, we obtain the spectral persistence bar codes describing the emergence of SCHs for each airline with respect to the others (see Figure 6). The induced SCH rankings are presented in Table 4.

6 Discussion and conclusion

We have introduced CSM as a generalization of both the notions of simplicial complexes and multilayer networks. We further introduced cross-homology to study their topology and defined the cross-Laplacian operators to detect more structures that are not detected by homology. Our goal here was to set up a mathematical foundation for studying higher-order multilayer complex systems.

10.3389/fcpxs.2023.1281714

TABLE 4 Ranking of the 10 most persistent SCHs for the diffusion bicomplexes associated with the European air transportation multiplex network.

1. $X^{Lufthansa \to Ryanair}$		2. $X^{Lufthansa \to Easyjet}$	
Airport	Rank	Airport	Rank
Frankfurt Airport	1	Frankfurt Airport	1
Munich Airport	2	Munich Airport	2
Düsseldorf Airport	3	Milan Malpensa Airport	3
Stuttgart Airport	4	Düsseldorf Airport	4
Larnaca Airport	5	Stuttgart Airport	5
Leipzig Halle Airport	5	Larnaca Airport	6
Geneva Airport	5	Leipzig Halle Airport	6
Athens Airport	5	Geneva Airport	6
Amsterdam Airport Schiphol	5	Athens Airport	6
Birmingham Airport	5	Amsterdam Airport Schiphol	6
3. $X^{Ryanair \to Lufthansa}$		4. $X^{Ryanair \to Easyjet}$	
Airport	Rank	Airport	Rank
London Stansted Airport	1	Bergamo Airport	1
Bergamo Airport	2	Dublin Airport	2
Dublin Airport	3	London Stansted Airport	3
Charleroi Airport	4	Madrid Barajas Airport	4
Paris Beauvais Airport	5	Rome Ciampino Airport	5
Porto Airport	6	Palma de Mallorca Airport	6
Tampere Airport	7	Ibiza Airport	7
Kaunas Airport	8	Bologna Airport	8
Zaragoza Airport	9	Girona Airport	9
Göteborg City Airport	10	Moss Airport, Rygge	10
5. $X^{Easyjet \to Lufthansa}$		6. $X^{Easyjet \to Ryanair}$	
Airport	Rank	Airport	Rank
Paris Charles de Gaulle Airport	1	Paris Charles de Gaulle Airport	1
London Stansted Airport	2	London Stansted Airport	2
Berlin Brandenburg Airport	3	Milan Malpensa Airport	3
London Luton Airport	4	Berlin Brandenburg Airport	4
Amsterdam Airport Schiphol	5	Belfast International Airport	5
Edinburgh Airport	6	London Luton Airport	6
Manchester Airport	7	Amsterdam Airport Schiphol	7
Rome Fiumicino Airport	8	Edinburgh Airport	8
Athens Airport	9	Newcastle Airport	9
Geneva Airport	10	Lyon-Saint Exupéry Airport	10

Nevertheless, through synthetic examples of CSM and applications in multiplex networks, we have shown that our framework provides powerful tools to reveal important topological features in multilayer networks and address questions that would not arise from the standard pairwise-based formalism of multilayer networks. We specially focused on the (0,0) cross-Laplacians to show how their

spectra quantify the extent to which nodes in one layer control topological structures in other layers in a multilayer network. Specifically, we saw that the spectra of these matrices allow detection of nodes from one layer that serve as inter-layer connecting hubs for clusters in the other layer; we referred to such nodes as SCHs. Such hubs vary in function of the eigenvalues, and they can be ranked according to their *spectral persistence* along the spectra of the cross-Laplacians. SCHs obtained from the largest eigenvalues (*principal cross-hubs* or PCHs) are those that interconnect the most important structures of the other layer. We should note that a PCH is not necessarily spectrally persistent, and two SCHs can be equally persistent but at different ranges of the spectrum. This means that, depending on the applications, some choices need to be made when ranking SCHs based on their spectral persistence. It might be the case that two SCHs persist equally long enough to be considered the most persistent ones, but that one persists through the first quarter of the spectrum, while the other persists through the second quarter of the spectrum so that none of them is PCH.

One can observe that the topological and geometric interpretations given for $\mathcal{L}_{0,0}^{(\mathrm{T})}$ and $\mathcal{L}_{0,0}^{(\mathrm{B})}$ can theoretically be generalized to the higher-order (k, l) cross-Laplacians as well. In other words, the spectra of these operators encode the extent to which higher-order topological structures (edges, triangles, tetrahedrons, and so on) control the emergence of higher-order clustering structures in the other layers. However, in practice, dealing with the higher-order cross-Laplacians could quickly become computationally heavy or infeasible. It would, however, be interesting to see how the (0,1) and (1,1) cross-Laplacians translate in real datasets involving intrinsic intra- and inter-layer triangles and tetrahedrons.

Finally, many recent advances in structural and functional neuroimaging and genomics are based on the analysis of complex network representations of the human brain. The proposed framework will enable us to analyze the intimate relationships between the brain structure, genomics, and functional representations within unified multilayered structures.

7 Methods

7.1 Cones, kites, and the (0,0) cross-Betti numbers

Let v_j^2 be a fixed vertex in V_2. A *kite from* V_1 *to* v_j^2 is an ordered tuple $(v_{i_1}^1, \ldots, v_{i_p}^1)$ of vertices in V_1 such that $\{v_{i_r}^1, v_{i_{r+1}}^1, v_j^2\} \in X_{1,0}$ for $r = 1, \ldots, p-1$. Such an object is denoted as $(v_{i_0}^1, \ldots, v_{i_p}^1 \leftarrow v_j^2)$. Beware that the vertices $v_{i_1}^1, \ldots, v_{i_p}^1$ do not need to be pair-wise connected in V_1. We observe the cross-triangles all pointing to v_j^2 that are pieced together in the form of an actual kite, as shown in Figure 7. In particular, if v_j^2 is the bottom face of a (1,0) cross-triangle $[v_i^1, v_k^1; v_j^2]$, then $(v_i^1, v_k^1 \leftarrow v_j^2)$ is a kite. If $(v_{i_1}^1, \ldots, v_{i_p}^1 \leftarrow v_j^2)$ is a kite, its *boundary* is the triple $(v_{i_1}^1, v_{i_p}^1, v_j^2) \in V_1^2 \times V_2$. Similarly, given a fixed vertex $v_i^1 \in V_1$, one can define a *kite from* V_2 *to* v_i^1 by a tuple $(v_{j_1}^2, \ldots, v_{j_{p'}}^2)$ of vertices in V_2 satisfying the analogous conditions. Such a kite will be denoted as $(v_i^1 \rightarrow v_{j_1}^2, \ldots, v_{j_{p'}}^2)$.

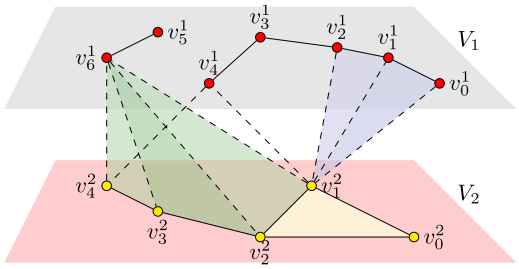

FIGURE 7
Two-dimensional crossimplicial bicomplex containing kites and cones. (v_0^1, v_1^1, v_2^1) is a kite from $V1$ to $v_1^2 \in V_2$ with boundary $(v_0^1, v_2^1, v_1^2) \in V_1^2 \times V_2$, and $(v_1^2, v_2^2, v_3^2, v_4^2)$ is a kite from V_2 to $v_6^1 \in V_1$ with boundary $(v_6^1, v_1^2, v_4^2) \in V_1 \times \in V_2^2$. The tuples (v_1^2, v_2^2, v_3^2), (v_1^2, v_2^2) and (v_2^2, v_3^2, v_4^2) are also kites from V_2 to v_6^1. Furthermore, there are three cones with bases in V_1: (v_2^1, v_4^1, v_1^2) is a closed cone with base $(v_2^1, v_4^1) \in V_1$ and vertex $v_1^2 \in V_2$, and (v_4^1, v_6^1, v_1^2) is an open cone with base $(v_4^1, v_6^1) \in V_1^2$ and vertex $v_1^2 \in V_2$. In addition, (v_4^1, v_6^1, v_4^2) is an open cone with base $(v_4^1, v_6^1) \in V_1^2$ and vertex $v_4^2 \in V_2$, and $(v_1^2, v_4^2, v_4^1) \in V_2^2 \times V_1$ is a closed cone with base $(v_1^2, v_4^2) \in V_2^2$ and vertex $v_4^1 \in V_1$. It follows from Theorem 7.1 that $\beta_{0,0} = (3, 1)$.

It is worth noting that if $(v_{i_1}^1, \ldots, v_{i_p}^1)$ is a kite from V_1 to v_j^2, then so is each tuple $(v_{i_r}^1, v_{i_{r+1}}^1, \ldots, v_{i_{r+q}}^1)$ with $1 \leq r$ and $r + q \leq p$.

By a *cross-chain* on a kite, we mean one that is a linear combination of the triangles composing the kite; in other words, a cross-chain on the kite $(v_{i_1}^1, \ldots, v_{i_p}^1 \leftarrow v_j^2)$ is an element $a \in C_{1,0}(X)$ of the form

$$a = \sum_{r=1}^{p-1} \gamma_r \left[v_{i_r}^1, v_{i_{r+1}}^1; v_j^2 \right], \tag{13}$$

where $\gamma_1, \ldots, \gamma_{p-1} \in \mathbb{R}$. In a similar fashion, cross-chains on a kite of the form $(v_i^1 \rightarrow v_{j_1}^2, \ldots, v_{j_{p'}}^2)$ are defined.

Now, given a pair (v_i^1, v_k^1) of vertices in the layer V_1 and the vertex $v_j^2 \in V_2$, we say that the triple $(v_i^1, v_k^1, v_j^2) \in V_1^2 \times V_2$ is a *cone with base* (v_i^1, v_k^1) *and vertex* v_j^2 if it satisfies the following conditions:

- $v_i^1 \sim v_j^2$ and $v_k^1 \sim v_j^2$, *i.e.*, $[v_i^1; v_j^2], [v_k^1; v_j^2] \in X_{0,0}$;
- the triple $(v_i^1, v_k^1, v_j^2) \in V_1^2 \times V_2$ is not the boundary of a kite from V_1 to v_j^2.

We also say that (v_i^1, v_k^1, v_j^2) is a *cone with the base in* V_1 *and the vertex in* V_2. In a similar fashion, one defines a cone with the base in V_2 and the vertex in V_1. We refer to Figure 7 for examples of cones.

An immediate consequence of a triple $(v_i^1, v_k^1, v_j^2) \in V_1^2 \times V_2$ being a cone is that the vertices $\{v_i^1, v_k^1, v_j^2\}$ are not (1,0) crossimplex. The vertices v_i^1 and v_k^1 might, however, be connected by a *horizontal path* of some length; when we mean that there might be a sequence of vertices $v_{i_0}^1, \ldots, v_{i_p}^1$ in V_1, not all of which form cross-triangles with v_j^2, and such that

$$v_i^1 \frown^{(1)} v_{i_0}^1 \frown^{(1)} \ldots \frown^{(1)} v_{i_p}^1 \frown^{(1)} v_k^1,$$

in which case, the cone is said to be *closed*; it is called *open* otherwise.

Cones in a crossimplicial bicomplex are classified by the top and bottom (0,0)-cross-homology groups of the bicomplex. Specifically,

we have the following topological interpretation of $\mathrm{H}^{(1)}_{0,0}(X)$, $\mathrm{H}^{(2)}_{0,0}(X)$, and hence, the (0,0) cross-Betti numbers.

Theorem 7.1. *The (0,0) cross-homology group* $\mathrm{H}^{(1)}_{0,0}(X)$ *(resp.* $\mathrm{H}^{(2)}_{0,0}(X)$*) is generated by the cross-homology classes of cones with bases in* V_1 *and vertices in* V_2 *(resp. with bases in* V_2 *and vertices in* V_1*). Therefore, the (0,0) cross-Betti number* $\beta^{(t)}_{0,0}$ *counts the cones with bases in* V_t*,* $t = 1, 2$.

Here, by the cross-homology class of the cone $(v^1_i, v^1_k, v^2_j) \in V^2_1 \times V_2$, for instance, we mean the top cross-homology of the (0,0) cross-chain $[v^1_k; v^2_j] - [v^1_i; v^2_j] \in C_{0,0}(X)$.

Proof. We prove the theorem for $\mathrm{H}^{(1)}_{0,0}(X)$ since the same arguments apply to $\mathrm{H}^{(2)}_{0,0}(X)$. Every cone (v^1_i, v^1_k, v^2_j) defines a non-trivial (0,0) cross-cycle; in other words, the difference of the corresponding cross-edges $[v^1_i; v^2_j] - [v^1_k; v^2_j] \in \ker\partial^{(1)}_{0,0}$. More generally, suppose we are given p cones $(v^1_{i_1}, v^1_{i_2}, v^2_j), (v_{i_2}, v^1_{i_3}, v^2_j), \ldots, (v^1_{i_{p-1}}, v^1_{i_p}, v^2_j)$ with bases in V_1 and all with the same vertex $v^2_j \in V_2$. Then, for all real numbers $\alpha_1, \ldots, \alpha_p$ such that $\sum_{r=1}^{p}\alpha_r = 0$, the cross-chain

$$b = \sum_{r=1}^{p} \alpha_r \left[v^1_{i_r}; v^2_j\right] \tag{14}$$

is clearly a (0,0) cross-cycle with a non-trivial cross-homology class, *i.e.*, $b \in \ker\partial^{(1)}_{0,0}$ and $b \notin \mathrm{im}\partial^{(1)}_{1,0}$. Conversely, let $b' \in \ker\partial^{(1)}_{0,0}$. We can write

$$b' = \sum_{m=1}^{M} \alpha'_m \left[v^1_{i_m}; v^2_{i_m}\right] \in C_{0,0}(X),$$

so that $\partial^{(1)}_{0,0}(b') = \sum_{m=1}^{M}\alpha'_m [v^2_{i_m}] = 0$. Then, either all the $v^2_{i_m}$ values are pair-wise different, in which case b' is the trivial cross-cycle; or there exist $p+1$ subsets $(\{m_{r,1}, \ldots, m_{r,M_r}\})_{r=1}^{p+1}$ of $\{1, \ldots, M\}$ such that

$$v^2_{i_{m_{r,1}}} = v^2_{i_{m_{r,2}}} = \cdots = v^2_{i_{m_{r,M_r}}}, \text{ for } 1 \le r \le p$$

and

$$v^2_{i_{m_{p+1,j}}} \neq v^2_{i_{m_{p+1,j'}}}, \text{ for all } j \neq j', 1 \le j, j' \le M_{p+1}.$$

It follows that

$$\sum_{j=1}^{M_r} \alpha'_{m_{r,j}} = 0, \text{ for each } r = 1, \ldots, p \tag{15}$$

and $\alpha'_{m_{p+1,j}} = 0$ for all $j = 1, \ldots, M_{p+1}$. Hence, we get the following general expression of a (0,0) cross-cycle:

$$b' = \sum_{r=1}^{p}\sum_{j=1}^{M_r} \alpha'_{m_{r,j}} \left[v^1_{i_{m_{r,j}}}; v^2_{i_{m_{r,1}}}\right], \tag{16}$$

where the coefficients satisfy (15). Furthermore, it is straightforward to see that $b' \in \mathrm{im}\partial^{(1)}_{1,0}$ if, and only if, for each $r = 1, \ldots, p$, there exists a permutation τ_r of $\{1, \ldots, M_r\}$ such that

$$\left(v^1_{i_{m_{r,\tau_r(1)}}}, \ldots, v^1_{i_{m_{r,\tau_r(M_r)}}} \leftarrow v^2_{i_{m_{r,1}}}\right)$$

is a kite. In that case, we get $b' = \partial^{(1)}_{1,0}(a)$, where

$$a = \sum_{r=1}^{p}\sum_{r=1}^{M_r-1} \gamma_{m_{r,j}} \left[v^1_{i_{m_{r,\tau_r(j)}}}, v^1_{i_{m_{r,\tau_r(j+1)}}}; v^2_{i_{m_{r,1}}}\right], \tag{17}$$

and where, for $r = 1, \ldots, p$, the coefficients $\gamma_{m_{r,j}}$ are given by

$$\begin{cases} \gamma_{m_{r,1}} &= -\alpha'_{m_{r,\tau_r(1)}} \\ \gamma_{m_{r,2}} &= -\alpha'_{m_{r,\tau_r(1)}} - \alpha'_{m_{r,\tau_r(2)}} \\ &\vdots \\ \gamma_{m_{r,M_r-2}} &= -\alpha'_{m_{r,\tau_r(1)}} - \alpha'_{m_{r,\tau_r(2)}} - \cdots - \alpha'_{m_{r,\tau_r(M_r-2)}} \\ \gamma_{m_{r,M_r-1}} &= \alpha'_{m_{r,\tau_r(M_2)}}. \end{cases} \tag{18}$$

This shows that trivial cross-homology classes in $\mathrm{H}^{(1)}_{0,0}(X)$ are given by cross-cycles obtained from cross-chains on kites, i.e., images of sums of cross-chains in the form of (13).

7.2 Inner product, cross-Laplacians, and harmonic cross-forms

We define the following maps on cross-forms:

$$\begin{array}{ccc} C^{k,l}(X) & \xrightarrow{\delta^{(1)}_{k,l}} & C^{k+1,l}(X) \\ \Big\downarrow{\scriptstyle \delta^{(2)}_{k,l}} & & \\ C^{k,l+1}(X) & & \end{array}$$

by the following equations:

$$\begin{aligned} \delta^{(1)}_{k,l}\phi([a]) &= \sum_{b\in\partial^{(1)}_a} \mathrm{sgn}\left(b, \partial^{(1)}_a\right)\phi([b]), \text{ and } \delta^{(2)}_{k,l}\phi([c]) \\ &= \sum_{d\in\partial^{(2)}_c} \mathrm{sgn}\left(d, \partial^{(2)}_c\right)\phi([d]), \end{aligned} \tag{19}$$

for $\phi \in C^{k,l}(X)$, $a \in X_{k+1,l}$ and $c \in X_{k,l+1}$.

Now, for each pair of integers (k, l), we choose inner products $\langle\cdot,\cdot\rangle_{k,l}$, $\langle\cdot,\cdot\rangle_{k+1,l}$ and $\langle\cdot,\cdot\rangle_{k,l+1}$ on the real vector spaces $C^{k,l}(X)$, $C^{k+1,l}(X)$ and $C^{k,l+1}(X)$, respectively. The *adjoint operators* $(\delta^{(1)}_{k,l})^*\colon C^{k+1,l}(X) \to C^{k,l}(X)$ and $(\delta^{(2)}_{k,l})^*\colon C^{k,l+1}(X) \to C^{k,l}(X)$ are determined by the following relations:

$$\begin{aligned} \langle\delta^{(1)}_{k,l}\phi, \psi\rangle_{k+1,l} &= \langle\phi, \left(\delta^{(1)}_{k,l}\right)^*\psi\rangle_{k,l}, \\ \langle\delta^{(2)}_{k,l}\phi, \psi'\rangle_{k,l+1} &= \langle\phi, \left(\delta^{(2)}_{k,l}\right)^*\psi'\rangle_{k,l}, \end{aligned} \tag{20}$$

for $\phi \in C^{k,l}(X)$, $\psi \in C^{k+1,l}(X)$, and $\psi' \in C^{k,l+1}(X)$.

Any weight w on X defines such inner products on cross-forms by the following setting:

$$\langle\phi, \psi\rangle_{k,l} := \sum_{a\in X_{k,l}} w(a)\phi(a)\psi(a), \text{ for } \phi, \psi \in C^{k,l}(X). \tag{21}$$

It can be seen that, with respect to such an inner product, elementary cross-forms form an orthogonal basis. Moreover, given a weight function w and such an inner product, we get the following by simple calculations using (20):

$$\left(\delta^{(1)}_{k,l}\right)^*\phi([a]) = \sum_{\substack{a'\in X_{k+1,l} \\ a\in\partial^{(1)}a'}} \frac{w(a')}{w(a)}\mathrm{sgn}\left(a, \partial^{(1)}a'\right)\phi([a']), \tag{22}$$

for $\phi \in C^{k+1,l}(X)$, $a \in X_{k,l}$. In addition, we obtain a similar formula for $(\delta^{(2)}_{k,l})^*$.

Definition 7.2. We define the following self-adjoint linear operators on $C^{k,l}(X)$ for all $k, l \geq -1$:

- the *top-outer* (k, l)*-cross-Laplacian* (or *TO-Laplacian of order* (k, l)

$$\mathcal{L}^{(\mathrm{TO})}_{k,l} := \left(\delta^{(1)}_{k,l}\right)^* \delta^{(1)}_{k,l},$$

- the *top-inner* (k, l)*-cross-Laplacian* (or *TI-Laplacian of order* (k, l)

$$\mathcal{L}^{(\mathrm{TI})}_{k,l} := \delta^{(1)}_{k-1,l}\left(\delta^{(1)}_{k-1,l}\right)^*,$$

- the *top* (k, l) *cross-Laplacian*

$$\mathcal{L}^{(\mathrm{T})}_{k,l} := \mathcal{L}^{(\mathrm{TO})}_{k,l} + \mathcal{L}^{(\mathrm{TI})}_{k,l},$$

- and similarly, the *bottom-outer* (k, l) *cross-Laplacian* (*BO-Laplacian of order* (k, l))

$$\mathcal{L}^{(\mathrm{BO})}_{k,l} := \left(\delta^{(2)}_{k,l}\right)^* \delta^{(2)}_{k,l},$$

- the *bottom-inner* (k, l)*-cross-Laplacian* (*BI-Laplacian*)

$$\mathcal{L}^{(\mathrm{BI})}_{k,l} := \delta^{(2)}_{k,l-1}\left(\delta^{(2)}_{k,l-1}\right)^*,$$

- and the *bottom* (k, l)*-cross-Laplacian*

$$\mathcal{L}^{(\mathrm{B})}_{k,l} := \mathcal{L}^{(\mathrm{BO})}_{k,l} + \mathcal{L}^{(\mathrm{BI})}_{k,l}.$$

The null spaces of these operators, defined as the following subgroups

$${}^{(s)}\mathcal{H}_{k,l} = \ker\mathcal{L}^{(s)}_{k,l} = \left\{\phi \in C^{k,l}(X) | \mathcal{L}^{(s)}_{k,l}\phi = 0\right\}, s = T, B,$$

are called the spaces of *harmonic top (resp. bottom) cross-forms* on X.

There is a one-to-one correspondence between cross-cycle classes and harmonic cross-forms on CSB X. In other words, we have the following group isomorphisms generalizing (Eckmann, 1944; Horak and Jost, 2013).

Lemma 7.3. *For* $s = 1, 2$ *and for all* $k, l \geq -1$, *we have*

$$\mathrm{H}^{(s)}_{k,l}(X) \cong \ker\left(\mathcal{L}^{(s)}_{k,l}\right), \tag{23}$$

where we have used the notations $\mathcal{L}^{(1)}_{k,l} = \mathcal{L}^{(\mathrm{T})}_{k,l}$ *and* $\mathcal{L}^{(2)}_{k,l} = \mathcal{L}^{(\mathrm{B})}_{k,l}$.

Proof. Let us prove this result for $s = 1$ (similar arguments apply to $s = 2$). First, notice that from the identification $C_{k,l}(X) = C^{k,l}(X)$, we obtain the following:

$$\mathrm{H}^{(1)}_{k,l}(X) = \ker\left(\delta^{(1)}_{k,l}\right)\Big/\mathrm{im}\left(\delta^{(1)}_{k-1,l}\right) \cong \ker\left(\delta^{(1)}_{k,l}\right) \cap \mathrm{im}\left(\delta^{(1)}_{k-1,l}\right)^{\perp}, \tag{24}$$

and the analog holds for $\mathrm{H}^{k,l}_{(2)}(X)$. Moreover, recall from linear algebra that if $E \xrightarrow{f} F$ is a linear operator on two vector spaces equipped with inner products, then $\ker(f^*f) = \ker f$. Indeed, we clearly have $\ker f \subset \ker(f^*f)$. Next, if $x \in \ker(f^*f)$, then $\langle f^*fx, y\rangle_E = \langle fx, fy\rangle_F = 0$ for all $y \in E$, which implies that $x \in \ker f$. In our case, we have $\delta^{(1)}_{k,l}\delta^{(1)}_{k-1,l} = 0$ and $(\delta^{(1)}_{k-1,l})^*(\delta^{(1)}_{k,l})^* = 0$; hence,

$$\begin{aligned}\mathrm{im}\left(\mathcal{L}^{(\mathrm{TO})}_{k,l}\right) \subset \mathrm{im}\left(\delta^{(1)}_{k,l}\right)^* \subset \ker\left(\delta^{(1)}_{k-1,l}\right)^* \subset \ker\left(\delta^{(1)}_{k-1,l}\left(\delta^{(1)}_{k-1,l}\right)^*\right)\\ \mathrm{im}\left(\mathcal{L}^{(\mathrm{TI})}_{k,l}\right) \subset \mathrm{im}\left(\delta^{(1)}_{k-1,l}\right) \subset \ker\left(\delta^{(1)}_{k,l}\right) \subset \ker\left(\left(\delta^{(1)}_{k,l}\right)^*\delta^{(1)}_{k,l}\right).\end{aligned}$$

Therefore,

$$\begin{aligned}\ker\mathcal{L}^{(\mathrm{T})}_{k,l} &= \ker\left(\left(\delta^{(1)}_{k,l}\right)^*\delta^{(1)}_{k,l}\right) \cap \ker\left(\delta^{(1)}_{k-1,l}\left(\delta^{(1)}_{k-1,l}\right)^*\right)\\ &= \ker\left(\delta^{(1)}_{k,l}\right) \cap \ker\left(\delta^{(1)}_{k-1,l}\right)^*\\ &\cong \ker\left(\delta^{(1)}_{k,l}\right) \cap \mathrm{im}\left(\delta^{(1)}_{k-1,l}\right)^{\perp},\end{aligned}$$

and the isomorphism (23) follows from (24).

It follows that the eigenvectors corresponding to the zero eigenvalue of the (k, l) cross-Laplacian $\mathcal{L}^{(s)}_{k,l}$ are representative cross-cycles in the homology group $\mathrm{H}^{(s)}_{k,l}(X)$. Henceforth, we see that in order to get the dimensions of the cross-homology groups $\mathrm{H}^{(s)}_{k,l}(X)$, it suffices to find the eigenspaces corresponding to the zero eigenvalues of $\mathcal{L}^{(s)}_{k,l}$. In other words,

$$\beta^{(1)}_{k,l} = \dim\ker\mathcal{L}^{(1)}_{k,l}, \text{ and } \beta^{(2)}_{k,l} = \dim\ker\mathcal{L}^{(2)}_{k,l}. \tag{25}$$

7.3 Matrix representations

Since the sets $X_{k,l}$ are finite, the vector spaces $C_{k,l}(X)$ and $C^{k,l}(X)$ are finite dimensional, and as we have seen, the latter has the elementary cross-forms e_a, $a \in X_{k,l}$ as orthogonal basis with respect to inner products defined from weight functions. So, the cross-Laplacian operators $\mathcal{L}^{(s)}_{k,l}, s = T, B$ can be represented as real square matrices of dimension $|X_{k,l}|\times|X_{k,l}|$ whose entries are indexed by elementary cross-forms e_a. In order to compute these matrix representations, we first need to give their formal expressions as linear operators. Thanks to (22), we get the following for $\phi \in C^{k,l}$, $a \in X_{k,l}$:

$$\begin{aligned}\left(\delta^{(1)}_{k,l}\right)^*\delta^{(1)}_{k,l}\phi([a]) &= \sum_{\substack{a'\in X_{k+1,l}\\ a\in\partial^{(1)}a'}} \frac{w(a')}{w(a)}\mathrm{sgn}\left(a,\partial^{(1)}_a\right)\left(\delta^{(1)}_{k,l}\phi\right)([a'])\\ &= \sum_{\substack{a'\in X_{k+1,l}\\ a\in\partial^{(1)}a'}} \frac{w(a')}{w(a)}\mathrm{sgn}\left(a,\partial^{(1)}a'\right)\sum_{b\in\partial^{(1)}a'}\mathrm{sgn}\left(b,\partial^{(1)}a'\right)\phi([b])\\ &= \sum_{\substack{a'\in X_{k+1,l}\\ a\in\partial^{(1)}a'}} \frac{w(a')}{w(a)}\mathrm{sgn}\left(a,\delta^{(1)}a'\right)\left[\mathrm{sgn}\left(a,\partial^{(1)}a'\right)\phi([a]) + \sum_{b\in\partial^{(1)}a', b\neq a}\mathrm{sgn}\left(b,\partial^{(1)}a'\right)\phi([b])\right]\\ &= \sum_{\substack{a'\in X_{k+1,l}\\ a\in\partial^{(1)}a'}} \frac{w(a')}{w(a)}\left[\phi([a]) + \sum_{b\in\partial^{(1)}a', a\neq b}\mathrm{sgn}\left(a,\partial^{(1)}a'\right)\mathrm{sgn}\left(b,\partial^{(1)}a'\right)\phi([b])\right].\end{aligned}$$

and

$$\begin{aligned}\delta^{(1)}_{k-1,l}\left(\delta^{(1)}_{k-1,l}\right)^*\phi([a]) &= \sum_{\substack{c\in X_{k-1,l}\\ c\in\partial^{(1)}_a}}\mathrm{sgn}\left(c,\partial^{(1)}a'\right)\sum_{\substack{a'\in X_{k,l}\\ c\in\partial^{(1)}a'}}\frac{w(a')}{w(c)}\mathrm{sgn}\left(c,\partial^{(1)}a'\right)\phi([a'])\\ &= \sum_{\substack{c\in X_{k-1,l}\\ c\in\partial^{(1)}_a}}\mathrm{sgn}\left(c,\partial^{(1)}_a\right)\left[\frac{w(a)}{w(c)}\mathrm{sgn}\left(c,\partial^{(1)}_a\right)\phi([a])\right.\\ &\quad\left.+\sum_{\substack{c\in\partial^{(1)}a'\\ a\neq a'}}\frac{w(a')}{w(c)}\mathrm{sgn}\left(c,\partial^{(1)}a'\right)\phi([a'])\right]\\ &= \sum_{\substack{c\in X_{k-1,l}\\ c\in\partial^{(1)}_a}}\frac{w(a)}{w(c)}\phi([a]) + \sum_{\substack{c\in X_{k-1,l}\, a'\in X_{k,l}\\ c=\partial^{(1)}a'\cap\partial^{(1)}_a}}\frac{w(a')}{w(c)}\mathrm{sgn}\left(c,\partial^{(1)}_a\right)\mathrm{sgn}\left(c,\partial^{(1)}a'\right)\phi([a']).\end{aligned}$$

In particular, when ϕ is an elementary cross-form e_b, $b \in X_{k,l}$, we obtain the following:

$$\mathcal{L}_{k,l}^{(\mathrm{TO})} e_b([a]) = \begin{cases} \frac{1}{w(a)}\deg_{TO}(a), & \text{if } a = b, \\ -\frac{w(c)}{w(a)}, & \text{if } a \neq b \text{ and } a \frown_c^{(1)} b, \\ & \text{and have same orientation,} \\ \frac{w(c)}{w(a)}, & \text{if } a \neq b \text{ and } a \frown_c^{(1)} b, \\ & \text{and have opposite orientations,} \\ 0, & \text{otherwise}, \end{cases}$$

and

$$\mathcal{L}_{k,l}^{(\mathrm{TI})} e_b([a]) = \begin{cases} w(a)\deg_{TI}(a), & \text{if } a = b, \\ \frac{w(b)}{w(d)}, & \text{if } a \neq b \text{ and } a \cup_{(1)}^{d} b, \\ & \text{and have same orientation,} \\ -\frac{w(b)}{w(d)}, & \text{if } a \neq b \text{ and } a \cup_{(1)}^{d} b \\ & \text{and have opposite orientations,} \\ 0, & \text{otherwise}. \end{cases}$$

It follows that the (e_a, e_b)-th entry of the matrix representation of the top (k, l) cross-Laplacian $\mathcal{L}_{k,l}^{(\mathrm{T})}$ with respect to the inner product defined from the weight function w is given by the following:

$$\left(\mathcal{L}_{k,l}^{(T)}\right)_{e_a,e_b} = \begin{cases} \frac{1}{w(a)}\deg_{TO}(a) + w(a)\deg_{TI}(a), & \text{if } a = b, \\ \frac{w(b)}{w(d)} - \frac{w(c)}{w(a)}, & \text{if } a \neq b,\ a \frown_c^{(1)} b \text{ and } a \cup_{(1)}^{d} b, \\ & \text{and have same orientation} \\ \frac{w(c)}{w(a)} - \frac{w(b)}{w(d)}, & \text{if } a \neq b,\ a \frown_c^{(1)} b \text{ and } a \cup_{(1)}^{d} b, \\ & \text{and have opposite orientations} \\ \frac{w(b)}{w(d)}, & \text{if } a \neq b,\ a \cup_{(1)}^{d} b,\ \text{same orientation}, \\ & \text{and not top – outer adjacent}, \\ -\frac{w(b)}{w(d)}, & \text{if } a \neq b,\ a \cup_{(1)}^{d} b,\ \text{opposite orientations}, \\ & \text{and not top – outer adjacent}, \\ 0, & \text{otherwise}. \end{cases} \tag{26}$$

It is clear that we get similar matrix representation for the bottom (k, l) cross-Laplacian $\mathcal{L}_{k,l}^{(\mathrm{B})}$.

Data availability statement

Publicly available datasets were analyzed in this study. These data can be found at: http://complex.unizar.es/~atnmultiplex/.

Author contributions

EM: conceptualization, data curation, formal analysis, investigation, methodology, software, validation, visualization, writing–original draft, and writing–review and editing. OA: writing–review and editing. HB: Funding acquisition, investigation, project administration, resources, supervision, validation, visualization, and writing–review and editing.

Funding

The author(s) declare financial support was received for the research, authorship, and/or publication of this article. This work was supported by the Natural Sciences and Engineering Research Council of Canada through the CRC grant NC0981.

Acknowledgments

The code used for visualizations and computations will be made available upon request.

Conflict of interest

The authors declare that the research was conducted in the absence of any commercial or financial relationships that could be construed as a potential conflict of interest.

Publisher's note

References

Benson, A. R., Gleich, D. F., and Leskovec, J. (2016). Higher-order organization of complex networks. *Science* 353 (6295), 163–166. doi:10.1126/science.aad9029

Bianconi, G. (2021). *Higher-order networks*. Cambridge University Press.

Boccaletti, S., Bianconi, G., Criado, R., Del Genio, C. I., Gómez-Gardenes, J., Romance, M., et al. (2014). The structure and dynamics of multilayer networks. *Phys. Rep.* 544 (1), 1–122. doi:10.1016/j.physrep.2014.07.001

Cardillo, A., Gómez-Gardenes, J., Zanin, M., Romance, M., Papo, D., Pozo, F. d., et al. (2013). Emergence of network features from multiplexity. *Sci. Rep.* 3 (1), 1344–1346. doi:10.1038/srep01344

De Domenico, M., Solé-Ribalta, A., Cozzo, E., Kivelä, M., Moreno, Y., Porter, M. A., et al. (2013). Mathematical formulation of multilayer networks. *Phys. Rev. X* 3 (4), 041022. doi:10.1103/physrevx.3.041022

Eckmann, B. (1944). Harmonische funktionen und randwertaufgaben in einem komplex. *Comment. Math. Helvetici* 17, 240–255. doi:10.1007/bf02566245

Flores, J., and Romance, M. (2018). On eigenvector-like centralities for temporal networks: discrete vs. continuous time scales. *J. Comput. Appl. Math.* 330, 1041–1051. doi:10.1016/j.cam.2017.05.019

Fortunato, S., and Hric, D. (2016). Community detection in networks: a user guide. *Phys. Rep.* 659, 1–44. doi:10.1016/j.physrep.2016.09.002

Goerss, P. G., and Jardine, J. F. (2009). *Simplicial homotopy theory*. Springer Science and Business Media.

Griffa, A., Ricaud, B., Benzi, K., Bresson, X., Daducci, A., Vandergheynst, P., et al. (2017). Transient networks of spatio-temporal connectivity map communication pathways in brain functional systems. *NeuroImage* 155, 490–502. doi:10.1016/j.neuroimage.2017.04.015

Hatcher, A. (2000). *Algebraic topology*. Cambridge: Cambridge Univ. Press.

Horak, D., and Jost, J. (2013). Spectra of combinatorial laplace operators on simplicial complexes. *Adv. Math.* 244, 303–336. doi:10.1016/j.aim.2013.05.007

Iacopini, I., Petri, G., Barrat, A., and Latora, V. (2019). Simplicial models of social contagion. *Nat. Commun.* 10 (1), 2485. doi:10.1038/s41467-019-10431-6

Kivelä, M., Arenas, A., Barthelemy, M., Gleeson, J. P., Moreno, Y., and Porter, M. A. (2014). Multilayer networks. *J. complex Netw.* 2 (3), 203–271. doi:10.1093/comnet/cnu016

Lim, L.-H. (2020). Hodge laplacians on graphs. *SIAM Rev.* 62, 685–715. doi:10.1137/18m1223101

Liu, X., Maiorino, E., Halu, A., Glass, K., Prasad, R. B., Loscalzo, J., et al. (2020). Robustness and lethality in multilayer biological molecular networks. *Nat. Commun.* 11 (1), 6043. doi:10.1038/s41467-020-19841-3

Lotito, Q. F., Musciotto, F., Montresor, A., and Battiston, F. (2022). Higher-order motif analysis in hypergraphs. *Commun. Phys.* 5 (1), 79. doi:10.1038/s42005-022-00858-7

Lucas, M., Cencetti, G., and Battiston, F. (2020). Multiorder laplacian for synchronization in higher-order networks. *Phys. Rev. Res.* 2 (3), 033410. doi:10.1103/physrevresearch.2.033410

Mac Lane, S. (1963). Homology. *Grundlehren der mathematischen Wissenschaften in Einzeldarstellungen mit besonderer Berücksichtigung der Anwendungsgebiete*. Springer Berlin, Heidelberg: Academic Press. doi:10.1007/978-3-642-62029-4

Majhi, S., Perc, M., and Ghosh, D. (2022). Dynamics on higher-order networks: a review. *J. R. Soc. Interface* 19 (188), 20220043. doi:10.1098/rsif.2022.0043

Mandke, K., Meier, J., Brookes, M. J., O'Dea, R. D., Van Mieghem, P., Stam, C. J., et al. (2018). Comparing multilayer brain networks between groups: introducing graph metrics and recommendations. *NeuroImage* 166, 371–384. doi:10.1016/j.neuroimage.2017.11.016

Moerdijk, I. (1989). *Bisimplicial sets and the group-completion theorem*. Dordrecht: Springer Netherlands, 225–240.

Newman, M. E. (2003). The structure and function of complex networks. *SIAM Rev.* 45 (2), 167–256. doi:10.1137/s003614450342480

Pedersen, M., Zalesky, A., Omidvarnia, A., and Jackson, G. D. (2018). Multilayer network switching rate predicts brain performance. *Proc. Natl. Acad. Sci.* 115 (52), 13376–13381. doi:10.1073/pnas.1814785115

Pilosof, S., Porter, M. A., Pascual, M., and Kéfi, S. (2017). The multilayer nature of ecological networks. *Nat. Ecol. Evol.* 1 (4), 0101. doi:10.1038/s41559-017-0101

Sánchez-García, R. J., Cozzo, E., and Moreno, Y. (2014). Dimensionality reduction and spectral properties of multilayer networks. *Phys. Rev. E* 89 (5), 052815. doi:10.1103/physreve.89.052815

Schaub, M. T., Benson, A. R., Horn, P., Lippner, G., and Jadbabaie, A. (2020). Random walks on simplicial complexes and the normalized hodge 1-laplacian. *SIAM Rev.* 62 (2), 353–391. doi:10.1137/18m1201019

Shi, D., Chen, Z., Sun, X., Chen, Q., Ma, C., Lou, Y., et al. (2021). Computing cliques and cavities in networks. *Commun. Phys.* 4, 249. doi:10.1038/s42005-021-00748-4

Solá, L., Romance, M., Criado, R., Flores, J., García del Amo, A., and Boccaletti, S. (2013). Eigenvector centrality of nodes in multiplex networks. *Chaos (Woodbury, N.Y.)* 23, 033131. doi:10.1063/1.4818544

Timóteo, S., Correia, M., Rodríguez-Echeverría, S., Freitas, H., and Heleno, R. (2018). Multilayer networks reveal the spatial structure of seed-dispersal interactions across the great rift landscapes. *Nat. Commun.* 9 (1), 140. doi:10.1038/s41467-017-02658-y

Vasilyeva, E., Kozlov, A., Alfaro-Bittner, K., Musatov, D., Raigorodskii, A., Perc, M., et al. (2021). Multilayer representation of collaboration networks with higher-order interactions. *Sci. Rep.* 11, 5666. doi:10.1038/s41598-021-85133-5

Wu, M., He, S., Zhang, Y., Chen, J., Sun, Y., Liu, Y.-Y., et al. (2019). A tensor-based framework for studying eigenvector multicentrality in multilayer networks. *Proc. Natl. Acad. Sci.* 116, 15407–15413. doi:10.1073/pnas.1801378116

Young, J.-G., Petri, G., and Peixoto, T. P. (2021). Hypergraph reconstruction from network data. *Commun. Phys.* 4 (1), 135. doi:10.1038/s42005-021-00637-w

Yuvaraj, M., Dey, A. K., Lyubchich, V., Gel, Y. R., and Poor, H. V. (2021). Topological clustering of multilayer networks. *Proc. Natl. Acad. Sci. U. S. A.* 118 (21), e2019994118. doi:10.1073/pnas.2019994118